

Formation of the large-scale structure of the Universe

V. N. Lukash, E. V. Mikheeva, A. M. Malinovsky*

Astro Space Center of Lebedev Physical Institute, Russian Academy of Sciences, Profsoyuznaya st. 84/32, Moscow, 117997, Russia

Abstract

In this review, the formation, evolution, and decay of the large-scale structure of the Universe is discussed in the context of observational data, numerical simulations, and the Cosmological Standard Model (CSM). Problems concerning measuring and interpreting cosmological parameters, determining the composition of matter, and normalizing density perturbation spectra are especially highlighted.

Contents

1	Introduction	2
2	What the structure is	3
3	Why galaxies form	5
4	Boundaries of homogeneity	10
5	The quasi-Friedmann equations	13

*Electronic address: Alexandr.M.Malinovsky@gmail.com

6	Dynamical properties of the structure	15
7	Anisotropic cold flows	19
8	How the collapsing flows form	23
9	How to measure dark energy	25
10	How to measure the Universe	29
11	Formation of galaxies in the inhomogeneous Universe	37
12	Mass function of relaxed halos	40
13	Modulation of galaxies by the large-scale structure	44
14	Normalization of scalar perturbations	50
15	Conclusions	55
16	Appendices	55

1 Introduction

This review describes the processes of generation, evolution, and degradation of structures – linear, quasilinear, and nonlinear – and relaxed halos of dark matter (DM) in the Universe, based on theoretical developments and comparisons with observations and numerical simulations. Special attention is paid to: (1) the characteristics of dark energy (DE) and methods of measuring it, (2) DE, which gravitationally affects the growth of cosmological inhomogeneities and drastically influences the dynamics of DM structure formation, and (3) questions of normalizing density perturbation spectra on the basis of observations of the Universe’s large-scale structure. We separately consider the current status of DM equilibrium halos (their internal structure, density distribution, rotation curves, etc.) in review [1].

Turning to the most challenging questions of physical cosmology, we do not attempt to highlight all aspects related to the formation and decay of large-scale structure in the Standard Model (in particular, we do not elaborate on the baryon history of the structure). Both reviews rely on the original

research of the authors and follow respective chapters of monograph [2]. Here, we propose a more complete account of the aforementioned topics, invoking new observations and comparisons to the theory, and avoiding detailed analytical manipulations whenever possible (all necessary theoretical results are formulated in the Appendices; the interested reader will find proofs in book [2]).

2 What the structure is

The Hubble flow (recession, rushing outward, expansion) of matter observed on large scales bears *no structure*: it is compatible with spatially homogeneous and isotropic field of distributions of density, pressure, velocities, and other characteristics of matter. The structure is, by definition, *inhomogeneous* and is associated with distortions of the Hubble flow that have evolved from initial seeding inhomogeneities of the flow metric under the action of gravitational field *gradients*, which influence the motion and distribution of matter in space (see Appendices A and B). Spatial gradients grow if scales decrease. Relatedly, one distinguishes between linear, quasilinear, and non-linear structures.

By the large-scale structure of the Universe is meant the observed inhomogeneous matter distribution which deterministically evolved from the initial small geometric scalar perturbations (the S-mode of cosmological perturbations) ‘imprinted’ in the gravitational potential of the Hubble flow.¹ The modern Universe exhibits a well-developed non-linear structure in the form of halos of galaxies, groups, and clusters at small scales ($R < 10$ Mpc), and shows a more regular, quasilinear distribution of matter on larger scales up to hundreds of megaparsecs, exemplified by superclusters and cosmological voids. There are numerous transition forms between nonlinear and quasilinear structures.

Gravitationally bound halos are distributed nonuniformly in the Universe. They are frequently observed in sheet-like formations – ‘walls’ whose trans-

¹These perturbations are also called adiabatic or growing adiabatic density perturbations. Theoretically, one may also conceive of primary perturbations coming from inhomogeneities in the matter composition under invariable gravitational potential (so-called isometric perturbations). There are, however, no observational data (within the error bars of the measurement) which indicate that a part of the initial conditions might be described by these perturbations.

verse size does not exceed 10 Mpc. A wall does not expand transversely and appears to be a nonlinear formation. It can be quasilinear along the other two more extended directions, continuing to expand along them. The walls themselves are inhomogeneous, and appear as a collection of elongated ‘filaments’ which may intersect, forming ‘nodes’ – the rich clusters of galaxies. The mean inhomogeneity scale in the Universe measures 10 Mpc (the density contrast variance in a sphere of this radius is close to 1, $\sigma_{10} \simeq 1$), varying locally by increasing in the vicinity of clusters, and decreasing away from them.

The observed structure is associated with the development of gravitational instability in nonrelativistic collisionless matter. Initial quasiisotropic expansion of matter is accompanied by the development of anisotropy. In regions of augmented density, the expansion of gravitating matter slows down, comes to rest, and is superseded by a collapse. The initial stage of collapse proceeds mainly along one of three directions and leads to self-crossings (caustics) and the formation of one-dimensional oppositely directed flows. Later on, the regions of matter self-confined by its gravitational field relax, gradually acquiring a spherical shape and forming multistream systems trapped by gravity – the halos of DM. These processes, both well understood and studied, are corroborated by numerical experiments simulating billions of collisionless gravitating particles (the N -body simulations), and agree largely with observations (see, for example, Refs [3, 4]).

Quasilinear structures (the density contrast $\delta_R < 1$ [see Eqn (62) in Section 13]) are subject to a rigorous analytical treatment since there is a small parameter enabling the machinery of perturbation theory in this case. There are two analytical approximations describing nonlinear formation – that of Zel’dovich [5] (exact in the one-dimensional case), and Press-Schechter [6] (exact in the spherical case). As indicated by numerical simulations, the Zel’dovich approximation describes well the large-scale matter distribution in regions where the collapse has just begun. In contrast, the Press-Schechter formalism pertains to fairly small scales and describes the distribution of virialized halos of DM.

3 Why galaxies form

We observe the state of the Universe billions of years after the Big Bang. On large scales, the expansion of matter follows Hubble's law, which does not make a distinction between spatial points of the medium because the relative recessional velocity $\delta\mathbf{V}$ of *any* two neighboring elements of matter is proportional to the proper distance $\delta\mathbf{r}$ between them:

$$\delta\mathbf{V} \equiv \frac{\partial\delta\mathbf{r}}{\partial t} = H\delta\mathbf{r}. \quad (1)$$

The proportionality coefficient $H = H(t)$ does not depend on the spatial coordinates or mutual location of these elements,² but depends on the proper physical time t . This law of matter expansion is preserved as a relict from the early history of the Universe, being, in essence, synonym of the notion of the Universe. It conceals all the information on the formation of the Universe and the seeds in its structure.

Even though H is independent of spatial coordinates x , the metric described by Eqn (1) is homogeneous and isotropic only *locally*,³ i.e., it still depends on $\mathbf{x} = x^i$ ($i = 1, 2, 3$). The Hubble flow (1) can be conceived of geometrically as a three-dimensional spatial (initially curved) hypersurface that uniformly stretches with time, preserving local isotropy at all spatial locations, with the factor of local stretching $a(t) \cdot \mathbf{a}_{ij}(\mathbf{x})$, where $a = a(t)$ and $\mathbf{a}_{ij} = \mathbf{a}_{ij}(\mathbf{x})$ are some smooth continuous functions of class C^2 .

Indeed let us assume by definition

$$H_i^j \equiv \dot{a}_{ik} a^{kj},$$

where a_{ij} and a^{ij} are direct and inverse symmetric positive definite matrices (the dot over a letter implies a partial derivative with respect to t). From

²The modern value is $H_0 \simeq 70 \text{ km s}^{-1} \text{ Mpc}^{-1}$.

³Summing up vectors of distances and velocities on the hypersurface $t = \text{const}$, one readily concludes that if law (1) holds true for a particular observer, this same law is then also valid for all other points with just the same coefficient H . This, however, *does not prove* the global homogeneity of space: we are dealing with a tautology, because an isotropic and homogeneous hypersurface is assumed *a priori* in this conjecture in the form of linear superposition of distances and velocities. Notice that the dependence of H on \mathbf{x} can manifest itself on scales in excess of the size of the observable Universe. The real scale of the Friedmann world – the region of homogeneity where the linear superposition of velocities is valid – exceeds the Hubble radius [see Eqn (7) below]. Finding it is a question of the accuracy of observational data.

Eqn (1) we understand that they admit the factorization

$$H_i^j = H \delta_i^j : \quad a_{ij} = a \cdot \mathbf{a}_{ij}, \quad a = \exp\left(\int H dt\right), \quad (2)$$

and correspond to the interval squared between medium points:

$$ds^2 = dt^2 - \delta \mathbf{r}^2 = dt^2 - a^2 g_{ij} dx^i dx^j, \quad (3)$$

$$\delta \mathbf{r} = \delta r_i \equiv a \cdot \mathbf{a}_{ij} dx^j, \quad g_{ij} = g_{ij}(\mathbf{x}) \equiv \mathbf{a}_{ik} \mathbf{a}_{lj} \delta^{kl}$$

[the Kronecker symbol here follows from Eqn (2)]. The converse statement is also true: differentiating $\delta \mathbf{r}$ from Eqn (3) with respect to time we recover Eqn (1) with $H = \dot{a}/a$. Relatedly, Eqns (1) and (3) are equivalent. They describe a *homogeneous* distribution of matter with a laminar Hubble flow such that the linear law of velocity superposition holds in the vicinity of any of its points. Passing from one spatial domain to another one, we have to redefine the rules of distance addition with regard to functions g_{ij} .

The modern value of the scale factor is taken to be equal to unity: $a \equiv (1+z)^{-1}$, where z is the redshift. In order to determine the boundaries of the Friedmann world, we expand g_{ij} in the Taylor series in some finite neighborhood of an arbitrary point:

$$g_{ij}(\mathbf{x}) = c_{ij} + k_0 c_{ijk} x^k + \frac{1}{2} k_0^2 c_{ijkl} x^k x^l + \dots, \quad (4)$$

where the coefficients k_0 and $c_{ij\dots}$ depend on the selected point, which we have placed at $\mathbf{x} = 0$ in this case, and k_0^{-1} is the scale of variation of trace γ_{ii} or the convergence radius $k_0 |\mathbf{x}| < 1$ within which the first term c_{ij} of the series exceeds the remaining sum. Since we are dealing with the form $g_{ij} dx^i dx^j$, we can always reduce c_{ij} to the unity form $c_{ij} = \delta_{ij}$ by an appropriate choice of coordinates and leave only nonvanishing coefficients $c_{ijk\dots}$. Expression (4) reduces then to the following:

$$g_{ij}(\mathbf{x}) = e^{-2q_0} (\delta_{ij} - 2\mathfrak{S}_{ij}), \quad (5)$$

where the irreducible scalar $q_0 = q(\mathbf{x})$ and small tensor $\mathfrak{S}_0 = \mathfrak{S}_{ij}(\mathbf{x})$ depend on \mathbf{x} and are close to zero at $\mathbf{x} \sim 0$ (the subscript ‘0’ on these functions implies the absence of the functional dependence on time).⁴

⁴To be fully rigorous, we have to add to the right-hand side of Eqn (5) some scalar

According to Eqn (5), the quantity $q(\mathbf{x})$ is defined up to an additive constant, and the difference in its values between distant points can be arbitrarily large. It is usually assumed that its mean value q_0 in the observed domain equals zero. In that case, the deviations of $q(\mathbf{x})$ from zero grow with the distance from the observer, and the upper bound on the Friedmann world is set by the condition

$$|q(k_0^{-1})| \sim 1. \quad (6)$$

This size is *a fortiori* larger than the radius of external curvature ($k_0 < H_0$), since $|q(\mathbf{x})| \ll 1$ within the scale of observable cosmology:⁵

$$q_H = |q(H_0^{-1})| \sim 10^{-4}. \quad (7)$$

Functions (5) encode information on the S and T modes of cosmological structure, which define the anisotropy of cosmic microwave background radiation (q_0 and \mathfrak{S}_0) and the seeds of galaxies (only q_0). It should be borne in mind that there are small corrections $\sim \nabla q_0 / \bar{H}$ to the metric (3) and that in this order the Hubble flows are weakly distorted. The gradients of q_0 may

$B_{,ij}$ and vector $\xi_{i,j}$ terms depending on \mathbf{x} (the comma in subscripts denotes a partial derivative over \mathbf{x}). These terms, however, lack physical sense and can be removed through coordinate transformations. Vector modes, as well as decaying branches of scalar (S) and tensor (T) perturbation modes, are incompatible with isotropic expansion (2). In contrast, the growing branches of S and T modes of geometric inhomogeneities are preserved in the form (3) on large scales and do not violate Hubble's expansion law (2). Actually, these 'frozen' gravitational potentials q_0 and \mathfrak{S}_0 constitute the seeds of cosmological structure. The decaying modes had already faded out before the formation of the Hubble flow began and certainly had been negligibly small by the beginning of the galaxy formation epoch.

⁵To derive relationship (7), one needs to make use of the Sachs-Wolfe formula [7]

$$\delta_{TSW} = q_{HZ}/5 \simeq 10^{-5}$$

and estimate q_H with the help of spectral integral

$$\langle q_H^2 \rangle = \int_{H_0}^{\infty} q_k^2 \frac{dk}{k} \sim q_{HZ}^2 \ln\left(\frac{k_{\text{eq}}}{H_0}\right) \simeq (2 q_{HZ})^2 \simeq 10^{-8},$$

where $q_{HZ} = q_{k \sim H_0}$ is the large-scale Harrison-Zeldovich spectrum [8, 9], and $k_{\text{eq}} = \dot{a}_{\text{eq}} \simeq 0.01 \text{ Mpc}^{-1}$ is the Hubble scale at the instant of time when radiation and matter densities are equal. Notice that relationship (6) is valid under the assumption of $|\mathfrak{S}_0(k_0^{-1})| \leq 1$. The function \mathfrak{S}_0 carries information on cosmological gravitational waves and partly on the pre-inflationary geometry of spacetime (the other part is hidden in the function q_0). It is not, however, related to galaxies and, according to observations, is much smaller than q_0 . We do not consider it in detail for these reasons.

evolve and disrupt the laminar flow at small scales, leading to its breakup into self-gravitating nonlinear clumps of matter.

We see that the early Universe is *deterministic* and all its motions can be considered in the framework of the Cauchy problem. By solving dynamical equations, we uncover the cause-consequence chain of events fully determined by the initial cosmological conditions (functions q_0 and \mathfrak{S}_0), which in fact gives rise to the cosmological time arrow.⁶

In summary, there are two regimes of matter organization, which are evolutionarily connected with each other and describe opposite processes: Hubble flows (large scales), and structure (small scales). From the GRT equations it follows that the metric (3)-(5) represents the leading term in the expansion of the *exact* solution in the small parameter

$$\frac{\beta k}{\bar{H}} < 1, \quad (8)$$

where β is the mean speed of sound in the medium, and k and $\bar{H} \equiv aH = \dot{a}$ are the spatial and Hubble frequencies, respectively. Of principal importance is the answer to the question of whether corrections to expression (3) grow or decay with time. The evolution leads to the *breakup* of existing Hubble flows in the first case, and to their *creation* in the latter.

The answer to this question depends on the sign of function $\bar{\gamma}$, where

$$\bar{\gamma} \equiv -\frac{\dot{\bar{H}}}{\bar{H}^2} = -\frac{d \ln \bar{H}}{d \ln a} = \frac{1}{2} \left(1 + \frac{3p}{\varepsilon} \right), \quad (9)$$

$$\gamma \equiv -\frac{\dot{H}}{H^2} = 1 + \bar{\gamma} = \frac{1}{2} \left(1 + \frac{p}{\varepsilon} \right).$$

Indeed, in the first order in gradients of q_0 we have [2]

$$q = q_0 + \int \delta_p \frac{da}{a}, \quad (10)$$

$$\mathbf{v}_{\text{pec}} = -\nu \nabla q_0, \quad \delta = g \Delta q_0, \quad \Phi = \phi q_0, \quad (11)$$

where $q = q(t, \mathbf{x})$ is the curvature potential [10, 11], ϕ is the gravitational potential, \mathbf{v}_{pec} is the peculiar velocity of matter motion relative to Hubble

⁶The time arrow can be violated in certain regions of spacetime where the relativistic effects are important (for example, in black holes or wormholes).

flow (1), and δ_p and $\delta_\varepsilon \equiv \delta$ are the comoving perturbations of total pressure (p) and matter energy density (ε) (see Appendices A and B). The growth factors $\nu = \nu(a)$, $g = g(a)$, and $\phi = \phi(a)$ depend only on time or the scale factor $a(t)$ respectively:

$$\nu = \frac{1}{a^2} \int \frac{da}{H}, \quad \phi = \gamma \bar{H}^2 g = 1 - \frac{H}{a} \int \frac{da}{H}. \quad (12)$$

A critical regime for the growth functions is the linear cosmological expansion for which

$$\bar{\gamma} = 0, \quad a \propto t.$$

In this case, ν , g , and ϕ are constant in time, and the evolution regimes mentioned above are separated: the Hubble flows are preserved at locations where they have existed, and no generation of new structures takes place.

For a decelerated expansion ($\bar{\gamma} > 0$), the functions $\nu(a)$ and $g(a)$ grow with time, a gravitational instability takes place, the initially laminar medium flows become disturbed, and the conditions arise for inhomogeneous structure formation on the side of small wavelengths (the function H monotonically decreases).

For an accelerated expansion ($\bar{\gamma} < 0$), the functions ν and g decay with time, and a new structure is not created but, in contrast, the build-up of Hubble flow and function $q(\mathbf{x})$ over an increasing range of scales $k_0 < k < \bar{H}$ continues (the function \bar{H} monotonically grows).

One may conclude that gravity in equal degree spawns two dynamical properties: repulsion (the generation of Hubble flows), and attraction (the generation of structure). Which of them will prevail depends on the equation of matter state [see Eqn (9)]: the inflation (repulsion, the generation of the Hubble flow) is realized for $(\varepsilon + 3p) < 0$, and the deceleration (attraction and the development of collapse) in the opposite case for $(\varepsilon + 3p) > 0$. Being inherent to GRT, both inflation and collapse occur for rather general initial distributions and properties of matter and lead to the emergence of *ordered* geometrical configurations on various scales – the Hubble flows, and nonlinear halos of matter.

The convergence of integral (10) at the lower limit assumes the dominance of initial adiabatic perturbations. If the isometric pressure scalar is neglected, the relationship between δ_p and δ takes a simple form: $\delta_p = \beta^2 \delta$, and the dynamics of scalar q obey the independent harmonic oscillator equation [10,

11] (see Appendix B)

$$\ddot{q} + \left(3H + 2\frac{\dot{\alpha}}{\alpha}\right)\dot{q} - \beta^2\frac{\Delta q}{a^2} = 0, \quad \alpha^2 = \frac{\gamma}{4\pi G\beta^2}. \quad (13)$$

where G is the Newtonian constant of gravitation. For small velocities of sound $|\beta| < 1$, the leading solution $q = q_0(\mathbf{x})$ continues into the causally connected domain [cf. expression (8)]. Spectral amplitudes of scalar curvature $q_0(k)$ in the post-recombination epoch and those of initial perturbations of the S-mode q_k are linked linearly:

$$q_0 = T(k) \cdot q_k, \quad (14)$$

where $T(k)$ is the transfer function of linear density perturbations that accounts for their evolution in the pre-galactic medium (for details, see Ref. [1]).

4 Boundaries of homogeneity

In the course of inflation in the early Universe, the *stretching* of the space-like hypersurface with the size of k_0^{-1} , already born by the preceding evolution, and the building-up of function $q(\mathbf{x})$ from the side of small scales $k \gg k_0$, which enter the zone $k < \bar{H}(t)$ from the microscopic region if $\dot{\bar{H}} > 0$ took place. In this case, the growth of scales $\propto a(t)$ takes over the Hubble radius $H^{-1}(t)$ (Fig. 1), all folds and irregularities of the initial hypersurface within k_0^{-1} are smoothed out, and the newly emerging small scales appear embedded into the already existing large-scale framework of the hypersurface being isotropized. We can say that in the course of accelerated expansion of matter the minimum comoving scale of the Hubble flow decreases.

The maximum size of Friedmann hypersurface k_0^{-1} is determined by the conditions at the beginning of inflation and, as follows from observations, exceeds the modern horizon ($k_0 < 2 \cdot 10^{-4} \text{ Mpc}^{-1}$, see Eqns (6) and (7)). The minimum size k_m^{-1} is linked to the end of the inflationary period of the Big Bang; it is certainly less than the size of the observable structure and compares to the wavelength of the background radiation quantum. In the process of post-inflationary decelerated matter expansion, the opposite process took place: the Hubble flow broke up from the side of small scales and its minimum size grew with time.

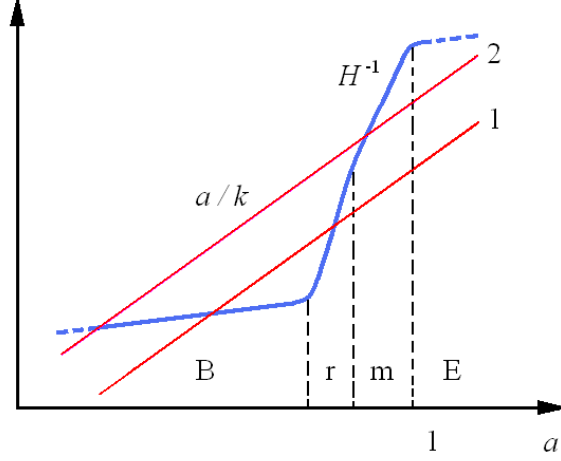


Figure 1: The Hubble radius H^{-1} (the line with bends) and sizes of perturbations $\propto a$ (inclined straight lines: 1 – a galaxy, 2 – a supercluster) as functions of a , from the Big Bang (B) to periods of radiation (r), DM(m), and DE (E).

In order to determine the minimum scale of current Hubble flow (1), we write down the first terms of metric expansion in the Lagrangian coordinates (t_c, \mathbf{x}) (the label ‘c’ of comoving time is dropped where possible):

$$ds^2 = (1 - 2\delta_p) dt^2 - \delta \mathbf{r}^2, \quad (15)$$

$$\delta \mathbf{r} = \delta r_i = ae^{-q}(\delta_{ij} - \mathbf{b} q_{0,ij}) dx^j, \quad (16)$$

and rewrite Hubble’s law in a more precise form [cf. Eqns (92) and (93) in Appendix A]

$$\delta V_i \equiv \frac{\partial \delta r_i}{(1 - \delta_p) \partial t} = H_{ij} \delta r^j, \quad (17)$$

where

$$H_{ij} = H (\delta_{ij} - \bar{h} q_{0,ij}), \quad \bar{h} \equiv \frac{\nu}{\bar{H}}, \quad \mathbf{b} = \int \bar{h} \frac{da}{a}. \quad (18)$$

Neglecting the effective speed of sound, we have at the lower boundary k_1 of the Hubble flow:

$$\delta \sim 1, \quad v_{\text{pec}} \sim \frac{\bar{H}}{k_1}, \quad q_0 \sim \frac{\bar{H}^2}{k_1^2} \ll 1. \quad (19)$$

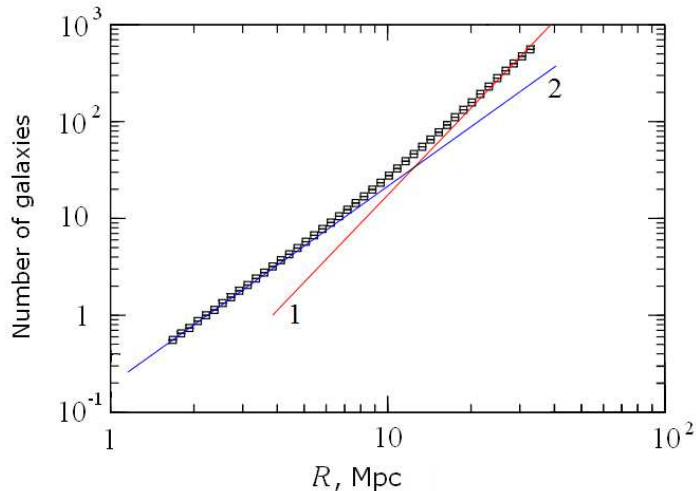


Figure 2: The spatially mean number of galaxies $N(R)$ in a sphere of radius R (according to Ref. [12]). The accuracy of power-law asymptotics is about 10%: 1 – $N \propto R^3$, the uniform distribution of matter, and 2 – $N \propto R^2$, the nonlinear structure of the Universe.

Recalling that the observed mean inhomogeneity scale $k_1 \sim 0.1 \text{ Mpc}^{-1}$ (Fig. 2), we obtain for the spectral amplitude of the curvature potential at the lower boundary of the current flow:

$$q_0(k_1) \sim 5 \cdot 10^{-6} \quad (20)$$

in agreement with the required value of the transfer function $T(k_1) \sim 0.1$.

Of interest is the question of determining experimentally the size k_0^{-1} of the Friedmann ‘background’ of our Universe. Doing so is possible, in principle. In fact, the scale k_0^{-1} need not be very large, because it is connected with the *last* period of accelerated expansion in the chain of inflationary stages of the Big Bang,⁷ and this period could be relatively short. In that case, k_0^{-1} can, in principle, exceed the radius of external curvature H_0^{-1} only slightly. In this situation, the total curvature potential $q_0(\mathbf{x})$ generated toward the end of inflationary explosion and determining the geometry of the observable world would be composed of *two* components: a *non-Gaussian*,

⁷Inflationary stages could have alternated with those dominated by matter which formed through the decay of intermediate short-lived inflatons.

strongly-correlated smooth part of size k_0^{-1} , linked to global pre-inflationary geometry, and small-scale (with respect to k_0^{-1}) ripples of a Gaussian field of inhomogeneities born in a quantum-gravitational way. The non-Gaussian component of density perturbations grows with an increase in the distance from the observer and manifests itself in the large-scale anisotropy of cosmic microwave background. The Gaussian perturbations do not decay as the scale is reduced, and are responsible for the formation of galaxies.⁸

The post-inflationary matter-dominated stage of decelerated expansion, accompanied by a reduction in the speed of sound, leads to the conditions for collapse at small scales, where a ‘window’ of gravitational instability opens. In contrast to the inflation, where initial conditions are forgotten, certain seed perturbations of curvature are required for the onset of collapse. They define domains of matter inflow and outflow.

Thus, the scale interval $k_1 < k \ll k_m$ in the modern epoch belongs to nonlinear cosmological structures, and the undisrupted quasi-Hubble flow of matter, albeit already distorted, still persists at scales $k < k_1$ (in the mean in the Universe).

5 The quasi-Friedmann equations

A weakly inhomogeneous Universe is described by the generalized Friedmann equation [2] (see Appendix A)

$$H_v^2 = \frac{8\pi G}{3} \varepsilon - \frac{\varkappa}{b^2}, \quad (21)$$

in which the geometrical scalar variables

$$H_v = H_v(t, \mathbf{x}) \equiv \frac{\dot{b}}{b} = \frac{1}{3} u^\mu_{;\mu}$$

(the semicolon indicates the covariant derivative) and $b = b(t, \mathbf{x})$ correspond to the local Hubble and scale factors of medium volume expansion, ε and u^μ

⁸The resultant amplitude of quadrupole anisotropy of relic radiation can be both lower and higher than the value expected for this extrapolation of the short-wave spectrum. This effect could explain the low quadrupole anisotropy of the cosmic microwave background radiation (if, of course, this anomaly is confirmed by future observations and rigorous data analysis).

are the total energy density and matter four-velocity, the small function

$$\varkappa = \varkappa(t, \mathbf{x}) \equiv \frac{2}{3} \Delta q \quad (22)$$

is the internal space curvature, and the dot above the symbols implies partial derivative with respect to the comoving time t_c . The time evolution of matter density obeys the conservation law

$$\dot{\epsilon} + 3H_v (\epsilon + p_v) = 0, \quad (23)$$

where p_v is the volume pressure [see Eqns (77) and (85)].

Equations (21) and (23) describing the evolution of the quasi-Friedmann Universe in geometrically invariant variables are valid for small spatial curvature $|\varkappa| \ll 1$ and include the zero the first orders of magnitude in deviations of weakly inhomogeneous geometry from Friedmann's one. These equations have a scalar form, although the geometry described by them is anisotropic [see Eqn (89)].

In order to solve Eqn (21) in the volume factor b , the defining scalar of curvature q must be known. Assuming that the small function q is known to us, we seek the solution in the form

$$H_v = H_c + \frac{\Delta\Phi - \Delta q}{3a\bar{H}}, \quad (24)$$

$$\varepsilon = \varepsilon_c + \frac{\Delta\Phi}{4\pi G a^2}, \quad p_v = p_c + \frac{\Delta S}{12\pi G a^2},$$

where $X_c \equiv X(t_c)$ are the background functions of comoving time, and Φ and S are arbitrary small functions of all coordinates. Substitution into Eqns (21) and (23) results in the *correct* coupling between scalars Φ and q [cf. Eqn (86)]:

$$\Phi = \frac{H}{a} \int a (\gamma q - S) dt, \quad (25)$$

with the arbitrary function S being not linked to the Einstein equations.

It should be emphasized that quasi-Friedmann Eqns (21) and (23) imply no constraints on the medium physical properties. Similarly to the original Friedmann equations, they link the spacetime curvature with total energy density, its time derivative, and the pressure of matter. As concerns the physical state of the matter, it needs to be considered only in the derivation of the equation of motion for the curvature scalar q (see Refs [2, 11] and Appendix B).

6 Dynamical properties of the structure

A physical reason for the emergence of nonlinear structure – the formation of galaxies from small primary curvature perturbations – is the gravitational instability of dark matter, most vigorously developing in the post-recombinant period of DM dominance.⁹ Since the initial pressure in nonrelativistic matter is low (relative particle velocities are close to zero at any point in space), the cold medium freely moves in own gravitational field of quasi-Hubble flow and the initially small peculiar velocities and the contrast of matter density grow with time on all scales. Consider at a greater length the dynamics of the quasi-Friedmann model at the linear stage of developing scalar inhomogeneities.

Let us turn to a simple model of the late Universe, which accounts only for nonrelativistic matter ‘m’ (with density inversely proportional to the local volume, $\rho_m \propto b^{-3}$) and dark energy ‘E’ of constant density ($\rho_E = \text{const}$). In this case, the mean speed of sound in the post-recombinant epoch is equal to zero [see Eqn (95), $\beta = \delta_p = 0$] and, consequently, the scalar q and spatial curvature \varkappa do not depend on time, and equation (21) simplifies. Multiplying it by $(b/H_E)^2$ and recasting in terms of dimensionless variables, we arrive at

$$\left(\frac{\dot{b}}{H_E}\right)^2 = f^2(b) - \hat{\varkappa}(\mathbf{x}), \quad (26)$$

where

$$f^2(b) \equiv \frac{8\pi G b^2}{3H_E^2} (\rho_m + \rho_E) = \left(\frac{c_m}{b} + b^2\right) \gtrsim 1, \quad (27)$$

$$q = q_0(\mathbf{x}) \equiv \frac{3}{2} H_E^2 \hat{q}, \quad \hat{\varkappa} = \hat{\varkappa}(\mathbf{x}) \equiv \frac{\varkappa}{H_E^2} = \Delta \hat{q}, \quad (28)$$

$H_E = H_0 \sqrt{\Omega_E} \simeq (5 \text{ Gpc})^{-1}$ is the Hubble constant of dark energy, $c_m \equiv \Omega_m/\Omega_E \simeq 0.4$ is the constant coefficient, one sixth of which is linked to

⁹It should be recalled that in the CSM the initial perturbations in composition are absent, the background curvature equals zero, and the parameters of the energy density of components take the following values: DE ($\Omega_E \approx 0.7$), nonbaryonic DM ($\Omega_M \approx 0.25$), baryons ($\Omega_b \approx 0.05$), and radiation ($\Omega_r \simeq 10^{-4}$). Notice that the 10% accuracy level of today’s observations does not yet enable distinguishing the cosmological constant and evolving DE. This witnesses in favor of its slow evolution and allows considering general models of DE in the form of expansions in terms of the small parameter $|w+1| \ll 1$, where the cosmological constant is the leading term in the series [see Eqn (44), $w \equiv p_E/\rho_E$].

baryons and the remaining 5/6 to DM (in this approximation, both components move together). Obviously, the function $f(b)$ attains a minimum $f_{\min} \simeq 1$ at $b_{\min}^{-1} \simeq 1.7$.

An arbitrary small function of spatial coordinates $\hat{\varkappa}$ describes the local normalized space curvature. We are interested in domains with the positive right-hand side of equation (26):

$$\hat{\varkappa}(\mathbf{x}) < 1. \quad (29)$$

In these domains, the matter density decreases monotonically with time [see Eqn (42) for details]. They comprise both superclusters ($\varkappa > 0$) and cosmological voids ($\varkappa < 0$).

The volume and background scale factors coincide at points $\varkappa = 0$ (the expansion anisotropy can be large in this case):

$$b = a(t) \equiv \frac{1}{1+z}, \quad H \equiv H_E \frac{f(a)}{a}. \quad (30)$$

where $f = f(a)$ is the growth factor of the Hubble velocity component

$$\mathbf{V}_H = f H_E \mathbf{x}. \quad (31)$$

In a general case, in the linear order in $\hat{\varkappa}$ we obtain

$$b = a \left(1 - \frac{1}{3} \hat{g} \hat{\varkappa} \right), \quad \delta_m = \hat{g} \hat{\varkappa}, \quad (32)$$

$$H_v = H \left(1 - \frac{1}{3} \hat{h} \hat{\varkappa} \right), \quad \hat{h} \equiv \frac{\bar{\nu}}{f} = \frac{\dot{\hat{g}}}{H}, \quad (33)$$

where $\delta_m = \delta$ is the density perturbation, $\hat{g} = \hat{g}(a)$ and $\bar{\nu} = \bar{\nu}(a)$ are, respectively, the growth factors of density perturbations and peculiar velocity (Fig. 3):

$$\hat{g} \equiv \frac{\gamma \bar{H}^2}{c_m} a = \frac{1}{c_m} \left(a - H \int_0^a \frac{da}{H} \right), \quad \bar{\nu} \equiv \frac{3}{2} H_E \nu = \frac{3 H_E}{2 a^2} \int_0^a \frac{da}{H}. \quad (34)$$

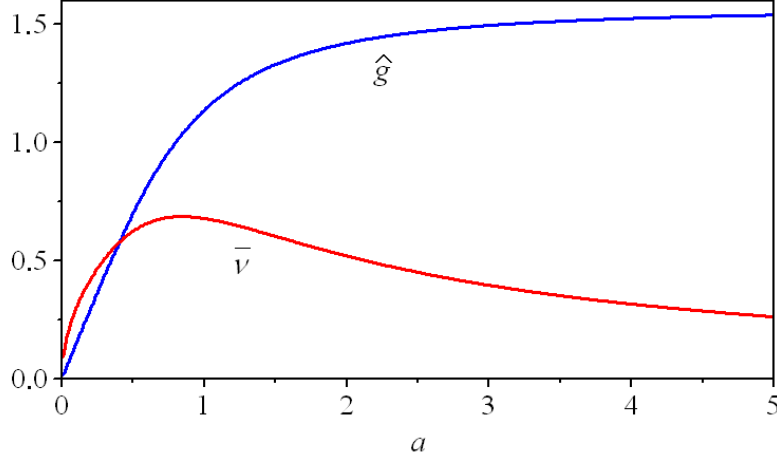


Figure 3: Growth factors of density $\hat{g}(a)$ and peculiar velocity $\bar{v}(a)$ [13].

For

$$\begin{aligned}
 a \ll 1 : & \quad \hat{g} \simeq \frac{3a}{2}, & \quad \bar{v} \simeq \sqrt{a}, \\
 a \gg 1 : & \quad \hat{g} = \hat{g}_{\max} \simeq 1.56, & \quad \bar{v} \simeq \frac{3}{2a}, \\
 a = 1 : & \quad \hat{g} \simeq 1.13, & \quad \bar{v} \simeq 0.67.
 \end{aligned}$$

Equations (26)-(34) describe quasi-Hubble anisotropic flows with the effective Hubble function H_v , which depends on the observer's location. In the modern epoch, the function \bar{v} shows a wide maximum, which is an indication of the period of most intense structure generation. The position of its maximum corresponds to $z \simeq 0.2$, the 90% level of its maximum value of $\bar{v}_{\max} \simeq 0.68$ is reached at $a \simeq 0.5$ and 1.4, and the 50% level is reached at $z \simeq 0.1$ and 4.

The current epoch is therefore that of *maximum* peculiar velocities, which will persist for the cosmological time [13]. The function \bar{v} will decrease twofold when the age of the Universe reaches 35 billion years. Only then will it be possible to speculate about the beginning of the epoch of the fading out of peculiar velocities in all space domains where $\hat{z} < 1$.

The function $\hat{h}(a)$ determining the deviation of the local Hubble factor from its background value is plotted in Fig. 4. The maximum $\hat{h}_{\max} \simeq 0.65$

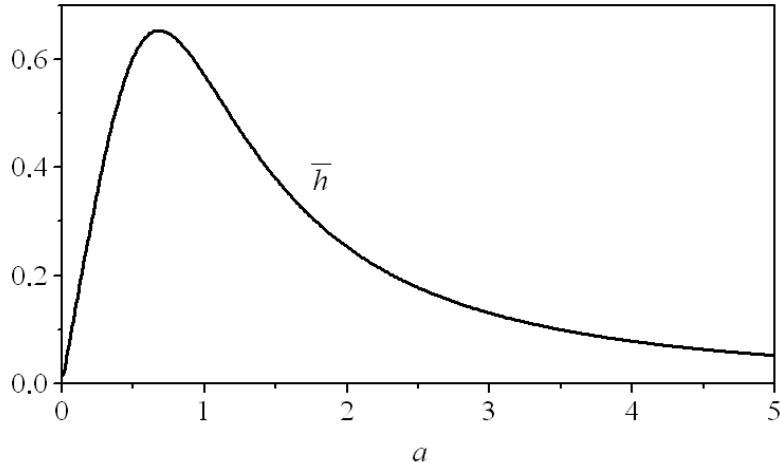


Figure 4: Function $\hat{h}(a)$ setting the distortion of the Hubble flow [13].

is reached at $z \simeq 0.4$, while the interval of the values of $\hat{h} > \hat{h}_{\max}/2$ is within the limits $a \in (0.1; 1.8)$, which corresponds to the range of the Universe's age, from 0.6 to 22 billion years. Figure 4 explicitly demonstrates that our Universe is at the stage where Hubble's expansion law is maximally distorted [$\hat{h}(a = 1) \simeq 0.87 \cdot \hat{h}_{\max} \simeq 0.57$], and that the recovery of Hubble flows in quasilinear domains of space will take about ten billion years.

We can conclude that the formation of large-scale structure in the Universe lasts for the period from 1 to 22 billion years after the Big Bang. The stage of suppression of the Hubble flow inhomogeneities, caused by the gravitational influence of DE, has not begun yet, although dark energy has been dominating in the density of matter for 3.5 billion years already. The delay hinges on the fact that the dynamic influence of DE on the structure generation in the Universe has just begun. Indeed, the characteristic time of this influence exceeds the current age of the Universe and amounts to $H_E^{-1} \simeq 17$ billion years.

7 Anisotropic cold flows

The field of peculiar velocities can conveniently be described by passing to the Eulerian coordinates in which the gravitational field is locally isotropic in a linear order in \varkappa at any space point (see Appendix B). The relationship between the Eulerian (\mathbf{y}) and Lagrangian (\mathbf{x}) coordinates we are interested in has the form

$$\mathbf{y} = \mathbf{x} + \hat{g} \hat{\mathbf{S}}, \quad (35)$$

where $\hat{\mathbf{S}} = \hat{\mathbf{S}}(\mathbf{x}) = -\nabla \hat{q}$ is the vector of displacement for an element of the medium relative to its unperturbed position, $\hat{\varkappa} = -\text{div} \hat{\mathbf{S}} = \Delta \hat{q}$. The Lagrangian coordinate \mathbf{x} does not vary here with time along the trajectory of the medium element and coincides with the Eulerian coordinate \mathbf{y} , as $t \rightarrow 0$. The growth factor for the displacement, $\hat{g} = \hat{g}(a)$, is simultaneously that for the density perturbation (32). The fact that the matter displacement relative to the laminar Hubble flow is factorized as a product of two functions (one dependent on time, and the other dependent on space coordinates) indicates that the rate of perturbation growth is the same for all wavelengths.

The net displacement of medium elements with respect to the unperturbed Hubble positions grows monotonically with time and amounts today to 14 Mpc. The mean net displacement will approach its limit value of about 22 Mpc (see Fig. 3) in the future, provided that the DE density does not change.

Using equation (35), we obtain the following representations for the interval on the Eulerian and Lagrangian grids:

$$ds^2 = (1 + 2\Phi) d\tau^2 - \mathbf{a}^2 d\mathbf{y}^2 = dt^2 - \mathbf{a}^2 (\delta_{ij} - 2\hat{g} \hat{q}_{,ij}) dx^i dx^j, \quad (36)$$

where $\tau = t - a \bar{\nu} H_E \hat{q}$, and $\mathbf{a} \equiv a(t) \cdot (1 - q) = a(\tau) \cdot (1 - \Phi)$ is the local scale factor [2]. The function $b(t, \mathbf{x})$ [see Eqns (21) and (32)] is proportional to the trace of the spatial part of the Lagrangian metric tensor, and the gravitational potential of density perturbations is equal to $\Phi = 0.6 \cdot \bar{\phi} q$, where

$$\bar{\phi} = \frac{5 c_m}{3 a} \hat{g} = \frac{5}{3} \left(1 - \frac{H}{a} \int \frac{da}{H} \right). \quad (37)$$

For $a \ll 1$, we get $\bar{\phi} = 1$. The temporal factor $\bar{\phi} = \bar{\phi}(a)$ of the gravitational potential decay under the action of DE is plotted in Fig. 5. The magnitude of $\bar{\phi}$ can serve as a *measure* of DE dynamic influence on the structure generation.

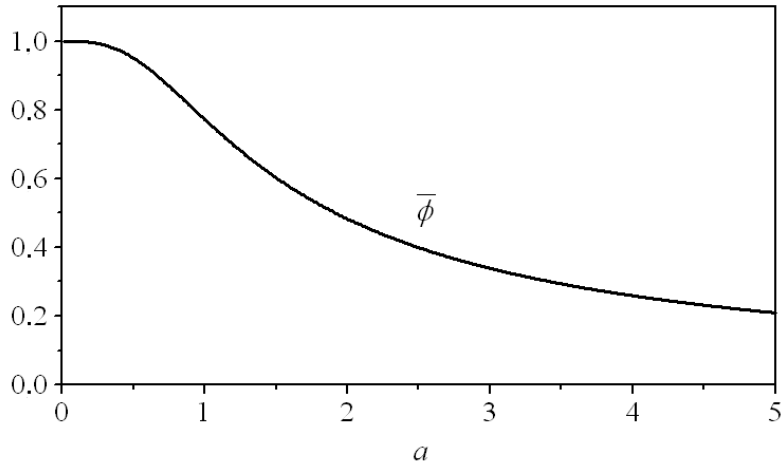


Figure 5: Decay of the gravitational potential $\bar{\phi}(a)$ of the large-scale structure of the Universe under the action of dark energy (see Ref. [2]).

By the current epoch, the potential $\bar{\phi}(a = 1) \simeq 0.77$ has already dropped by 23% off its constant value in the matter-dominated phase.

Interval (36) determines the physical Eulerian coordinate of medium element $\mathbf{r} = \mathbf{a}\mathbf{y} \simeq a\mathbf{y}$ (cf. Eqn (105)). Differentiating \mathbf{r} with respect to the proper time, we arrive at the following formula for the peculiar matter velocity:

$$\mathbf{v}_{\text{pec}} \equiv \dot{\mathbf{r}} - H\mathbf{r} = \hat{g}'\hat{\mathbf{S}} = \bar{\nu}H_{\text{E}}\hat{\mathbf{S}}. \quad (38)$$

Expression (38) coincides with the definition of 3-velocity as the spatial component of the 4-velocity of matter in the Eulerian reference frame:

$$\mathbf{v}_{\text{pec}} = -\frac{\partial t}{a\partial\mathbf{y}} = -\bar{\nu}H_{\text{E}}\nabla\hat{q} = -\frac{\nabla\mathbf{q}}{\bar{H}}.$$

Thus, the quantity $\bar{\nu}$ featuring in Eqn (33) is indeed the growth factor for the peculiar velocity.

According to Eqn (38), the total velocity of matter is defined as

$$\mathbf{V} = H\mathbf{r} + \mathbf{v}_{\text{pec}}.$$

The first component $H\mathbf{r}$ describes the Hubble velocity of the *nonuniform* Universe. It can also be split into two parts. One of them, $\mathbf{V}_H = \bar{H}\mathbf{x}$ [see

Eqn (31)], is connected with the homogeneous component of density, and the other, $\hat{g} \bar{H} \hat{\mathbf{S}}$, is connected with the perturbed one. The growth factor for the second component is proportional to the growth factor \hat{g} for density perturbations, whereas the peculiar velocity is $\propto \hat{g}'$.

We turn now to local flows of matter. In regions of the inhomogeneous Universe constrained by the condition (29), the flows of matter are described by the tensor field $H_{ij} = H_{ij}(t, \mathbf{x})$ generalizing the function $H(t)$ of the Friedmann model. Indeed, as follows from relationship (35), the coordinate distance between nearby points of the medium at time moment t is given by

$$\delta y_i = (\delta_{ij} - \hat{g} \hat{q}_{,ij}) \delta x^j. \quad (39)$$

Differentiating the physical distance $\delta \mathbf{r} = \mathbf{a} \delta \mathbf{y}$ over time, we obtain the field of pairwise velocities:

$$\delta V_i \equiv \frac{\partial}{\partial t}(\delta r_i) = H_{ij} \delta r^j, \quad (40)$$

$$H_{ij} = H \delta_{ij} - \dot{\hat{g}} \hat{q}_{,ij} = H \left(\delta_{ij} - \hat{h} \hat{q}_{,ij} \right).$$

The trace of the tensor field represents the volume Hubble function $H_v = H_{ii}/3$ [see Eqn (33)]; however, the tensor H_{ij} itself is strongly anisotropic. The anisotropy of local expansion (variations of projections of H_{ij} onto the radial directions emanating from the given point \mathbf{x}) has the same order of magnitude as the deviations of H_v from the mean value of the Hubble parameter H . At the boundary of quasilinear regions (29), these variations reach 100% (up to a point of stopped expansion in some directions). For example, in the vicinity of the Local Group, at a distance in excess of 2 Mpc from its barycenter, the principal values of the Hubble tensor are $H_{ij} = \text{diag}(48, 62, 81) \text{ km c}^{-1} \text{ Mpc}^{-1}$ (Fig. 6).

The field H_{ij} describes regular cold flows of matter. It is noteworthy that Eqn (40) is valid under the assumption that the distance between galaxies is small, below the correlation radius of the two-point correlation function for the displacement vector. For different projections of this vector relative to the direction of $\delta \mathbf{y}$, the correlation radius varies from 15 to 50 Mpc. The deviations from the velocity field (40) grow with distance. The spectrum of cosmological velocity perturbations is shaped namely in this manner: it decays toward shorter wavelengths for $k > 10^{-2} \text{ Mpc}^{-1}$ (see, for detail, Ref. [1]). For this reason, random deviations from mean velocities (40) in this range grow with an increase in scale.

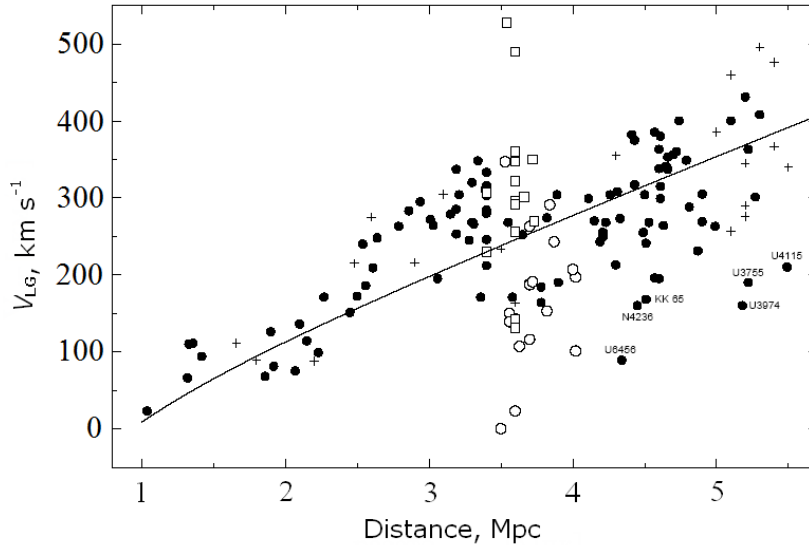


Figure 6: Radial velocities $V(r)$ of galaxies in the vicinity of the Local Group according to data of Ref. [14]. Different symbols correspond to different galaxy types, and distances to galaxies are given relative to the barycenter of the Local Group.

It should be kept in mind that deviations from dependence (40) amount to $\sim 40 \text{ km c}^{-1}$, i.e., about 25% of the mean velocity (see Fig. 6) at a distance of $\sim 2.5 \text{ Mpc}$ from the barycenter of the Local Group. At the same time, the total peculiar velocity of the Local Group relative to the cosmic microwave background radiation comprises 600 km c^{-1} . The scales of inhomogeneities responsible for so high velocities are in the interval from 15 to 70 Mpc.

We see that the standard theory of the Universe's structure formation encounters no difficulties in explaining the observed motions of matter in quasilinear regions of the Universe ($\hat{\chi} < 1$). The local flows are regular, smooth, and strongly correlated. The smallness of random galaxy velocity deviations from mean cold flow rates is explained by the shape of the initial spectrum of spatial density perturbations. These flows bear the quasi-Hubble character at small distances, preserving its main features: the flows are cold and radial, and the speed of galaxy recession is proportional to distance. However, the Hubble 'constant' depends on the observer position and the direction in space. We have already mentioned the neighborhood of the Local

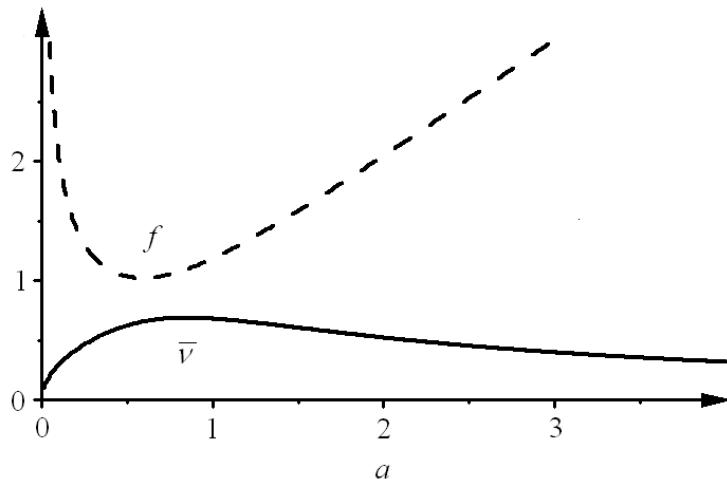


Figure 7: Growth factors of Hubble $f(a)$ (dashed line) and peculiar $\bar{v}(a)$ (solid line) velocities of matter [2]; $a = 1$ at $z = 0$.

Group as an example. The principal values of the Hubble tensor H_{ij} at a distance of several megaparsecs from its barycenter are related as 3 : 4 : 5.

As the radius grows, the deviations of galaxy velocities from the mean correlated flow rates increase too, beginning to saturate from distances of about 10 Mpc, which corresponds to the minimum correlation radius at which deviations of velocities reach the order of magnitude of the Hubble velocity proper. The deviations do not grow further, whereas the Hubble velocities continue to grow. At large distances, the flow of matter approaches the ideal Hubble law (1).

8 How the collapsing flows form

As shown earlier, dark energy, though not a component of structure, cardinally influences the structure generation rate and the history of galaxy formation. Figure 7 illustrates the behavior of growth factors of Hubble and peculiar components of matter velocity at the quasilinear stage of evolution. Because of the peculiar velocity growth, the expansion in certain regions of the Universe turns into a collapse which starts in certain directions and proceeds then toward the formation of gravitationally confined halo systems

with various masses. The spectrum of initial perturbations is shaped so that increasingly larger masses may collapse at later time moments (see also Ref. [1]).

If DE were absent, the Hubble velocity would continue to decrease with time, and the peculiar velocity would continue to grow. As a result, in any spatial domain where at least one of three principal values of tensor $\hat{q}_{,ij} = \text{diag}(\lambda_1, \lambda_2, \lambda_3)$ is positive [for example, $\lambda_1 > 0$, where $\lambda_1 \geq \lambda_2 \geq \lambda_3$; see Eqn (35)], sooner or later there will come an instant when the negative peculiar velocity in this direction becomes equal to Hubble's one and the expansion is halted [the principal value H_{11} turns to zero; see Eqn (40)]. In this case, the gravitational confinement of matter and its subsequent collapse ensue. However, because of the dynamical influence of DE not all domains succeed in evolving into the collapse stage: the Hubble velocity reaches a minimum at $z \simeq 0.7$, and then increases sharply as $\propto a$ [see Eqn (31)], whereas the peculiar velocity saturates and then slowly decreases (see Fig. 7). With account for DE influence, the process of galaxy formation resembles a fire burned out and lacking new firewood.

Thus, the nonlinear structure has a chance to form in those spatial zones where condition (29) is violated, namely

$$\hat{\chi} = \lambda_1 + \lambda_2 + \lambda_3 > 1. \quad (41)$$

Notwithstanding the threshold character of this inequality, it does not imply that regions occupied with nonlinear structures are topologically compact. Indeed, λ_3 (or $\lambda_{2,3}$) can appear to be negative, and then the expansion of matter will continue in that direction (or directions).

How can the transition from the quasilinear stage to the collapse phase be described? The answer is surprisingly simple: solution (35) can analytically be continued up to the first self-crossing ($\delta y_1 = 0$) and even further by 'matching' the arising multistream flows across caustics (the Zel'dovich approximation [5]).

This analytical approximation leads to correct qualitative conclusions, while quantitative deviations from the real evolution (until the first self-crossing) do not exceed 20-30% according to different criteria. The success of the approach, which is so simple, hinges on the potential q being small under cosmological conditions (the formation of black holes is exponentially suppressed). Moreover, the solution (35) proves to be exact in the nonlinear *one-dimensional* case, and namely this variant of initial collapse development is most typical in the Universe.

Relatedly, when computing the quantitative characteristics of a newly forming nonlinear structure – distribution functions for cosmological voids, superclusters, filaments, etc., mean distances between the walls, nodes, etc., correlation functions, evolution based on redshifts, and so on – one can rely on linear perturbations and their Gaussian statistics because solution (35) is naturally set by the field of small initial density inhomogeneities.

We give below two examples. First of all, we can exactly specify those domains where caustics fail to form, i.e., the expansion continues forever:

$$\lambda_1 < \hat{g}_{\max}^{-1} \simeq 0.6. \quad (42)$$

As long as density perturbations remain small, the two conditions (29) and (42) are equivalent. Condition (29), however, by no means ensures the absence of collapse: if $\lambda_1 > 0.6$, this direction, even if only in the future, will turn to the collapse. In a similar way, we can refine the density field. From relationship (35) we obtain the comoving matter density

$$\rho_m(\eta, \mathbf{x}) = \frac{c_m \rho_E}{a^3 \det(\delta y_i / \delta x_j)} = \frac{c_m \rho_E}{a^3 (1 - \hat{g} \lambda_1) (1 - \hat{g} \lambda_2) (1 - \hat{g} \lambda_3)}.$$

Formula (32) follows obviously from the last one for $\hat{g} \ll 1$.

We will return to nonlinear structures in the subsequent sections, and now proceed with the measurements of DE.

9 How to measure dark energy

DE can be measured only by means of observational cosmology. Its detection in the laboratory (similarly, for example, to attempts at laboratory detection of dark matter) seems to be implausible because this ever-penetrating substance (field) only weakly interacts with all objects, be they interiors of stars, compact objects, the early Universe, or others, during the entire world history known to us. Only indirect measurement methods are possible. Luckily, they have already proven their efficiency and led to impressive results – the discovery of DE proper.

What does it mean to measure DE? The answer to this question is hinted at by cosmology. The known constraints on the main DE parameter, viz.

$$|1 + w| < 0.1 \quad (43)$$

(see, for example, Ref. [15]) point to the constancy of function $w \equiv p_E/\varepsilon_E \approx \text{const}$ both in time and in space. Condition (43) simplifies the approach to DE detection to some extent. The DE clustering effects are of small significance and escape detection at the current level of technological development.

Today, we can only discuss actual experiments dealing with the dependence of function w on time: $w(a)$. Taking into account the slowness of evolution, this function can be replaced by the set of constant coefficients c_n of its Taylor expansion around -1 :

$$w(a) = -1 + c_0 + c_1\Delta a + \dots + c_n \frac{(\Delta a)^n}{n!} + \dots, \quad (44)$$

where $\Delta a = 1 - a \equiv z(1 + z)^{-1}$. At the current level of knowledge, the physical information on DE available to us is stored in these coefficients. From inequality (43) we find $|c_n| < 0.1$. Certainly, first of all, a pending question is the measurement of c_0 and the leading expansion coefficients. Theoretical predictions, based on connections of c_n with physical parameters of models (φ_0 , m , and others), in no way discriminate their range of values. Hence, the question hangs solely on the possibility of experimental assessment of the function $w(a)$.

We single out three main ways of measuring $w(a)$: structural, dynamical, and geometrical. Let us consider briefly each of them. We have already discussed the structural method earlier. Without being a part of the structure, DE cardinally influences the galaxy formation rate. It is the structural argument that has led to the discovery of the DE phenomenon. The achievements of all of 20th-century astronomy established that only a small fraction of mass enters the large-scale structure of the Universe. The remaining largest part is, hence, contained in the form of unstructured DE. Figures 3-5 and 7 depict the growth curves for the seeds of structure in the case where all $c_n = 0$. For c_n different from zero, the evolution curves will deform, as can easily be computed with the help of the GRT. The point, therefore, lies in maximally precise observational measurements of real growth functions and in determining the parameters c_n with their help.

How can the growth curves be measured accurately? Unfortunately, one can hardly rely on the traditional astronomical methods of observing the compact sources at different wavelengths (stars, including supernovae, quasars, galaxies, clusters, and so forth) and assessing based on these data the quantitative characteristics of inhomogeneous matter distributions in space and time. The obstacle here is uncontrolled nonlinear effects of coupling between

density distributions of matter and light. They, eventually, make impossible the recovery of mass distribution, based on the luminosity of its baryonic component, with necessary accuracy.

The true breakthrough in the structural method of detection of DE properties can be expected from dynamical measurements which are sensitive to gradients of total gravitational potential. An example can be furnished by statistical measurements of background galaxies weakly lensed by nearby structures, but even here barriers are met. The point is that the retrieved surface density of total mass (for a given redshift), which is the final product of the method, is still insufficient for a successful comparison with theory. Notably, we are not in a position to compute the contribution from baryons with necessary accuracy because of their complex interaction with light (shock waves, stellar formation, supernovae, dissipation, ultraviolet background, ionization, cooling, and so on).

In today's discussion of maximally precise methods of measuring DE, the case in point is largely the exploration of *linear and quasilinear* structures because, in this case, there is a well understood and fully controllable theory. An example of a breakthrough in this field is furnished by measurements of anisotropy and polarization of cosmic microwave background radiation (CMBR) that has led to the creation of CSM. A similar breakthrough is also possible by further developing this model based on accurate measurements of cosmological parameters, including those of DE.

This breakthrough can be provided by *any* statistical measurements of large-scale peculiar velocities of matter, inhomogeneities of gravitational potential, and distributions of matter density. In the first case, we have to do with the Doppler effects pertaining to the motion of matter [16, 17], and the measurement of the field of peculiar velocities based on proper motions of galaxies on the celestial sphere [18]. In the second case, it is the retrieval of gravitational potential with the help of the weak lensing effect, but this time at larger scales, where self-crossing of streams of matter is absent and the contribution from baryons is easily assessed [19]. In the third case, we are dealing with quantitative distribution of structures as a function of redshifts, and the detection of baryonic acoustic modulation of the density perturbation spectrum (see, for example, Ref. [20]).

Staying on this path, we arrive at the dynamical method of measuring DE by virtue of the Sachs-Wolfe integral effect. The influence of DE induces an *additional* source of the CMBR anisotropy, related to the decay of the linear gravitational field in the current epoch (see Fig. 5). By measuring this effect,

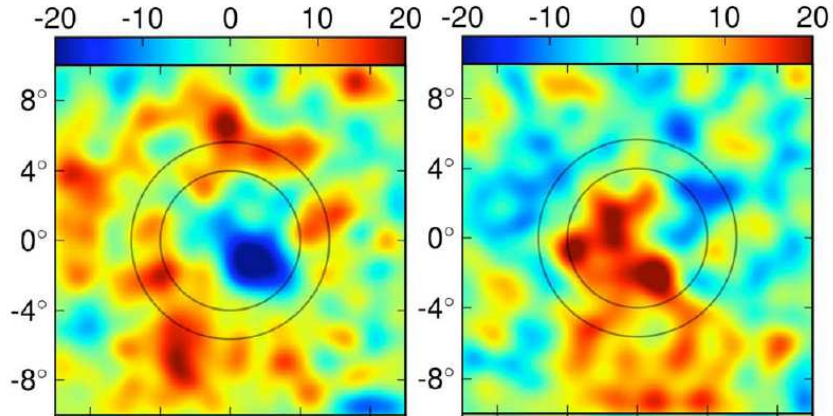


Figure 8: Superimposed portions of a cosmological microwave background map, which are projected onto 50 voids (a) and 50 superclusters (b) ~ 100 Mpc (4°) in size, based on results of Ref. [21]. The colorbar of the anisotropy of cosmic microwave background radiation (the insert at the top) is in microkelvins.

one can exactly determine the properties of DE, as has already been done when determining the parameters of the early Universe from measurements of the anisotropy parameters of CMBR in the recombination epoch. Quantitatively, here we need to raise the measurement accuracy only by one order of magnitude.

The dynamical integral effect predicts the existence of a cross-correlation between two celestial maps – those of CMBR anisotropy, and the large-scale structure of the Universe. Figure 8 shows superimposed regions of CMBR maps, projecting onto 50 voids (Fig. 8a) and 50 superclusters (Fig. 8b) set apart from the galaxy distribution in the SDSS catalogue. The mean size of voids/superclusters is about 100 Mpc. Summation of respective regions with reduced and increased densities of matter is performed to amplify the cross-correlation signal against the background of a random field of primary perturbations. We observe an apparent valley in the temperature of relic radiation (a cold spot) in directions towards voids, and a hot spot of the appropriate angular size in the direction towards superclusters, in full agreement with theoretical predictions.

These are only the first results which demonstrate the correspondence with what we already know well from the structural studies. Here, however,

the *precise* cosmological information is encoded; it can be deciphered in future observations and used to construct a more precise model of the Universe. Realization of this wonderful opportunity requires two exact maps of linear cosmological perturbations: the anisotropy of CMBR, and the gravitational potential of the large-scale structure. All this is possible at the already available technological level, but hinges on building new-generation telescopes, both ground-based and operating in space.

10 How to measure the Universe

Impressive successes in exploring the Universe rely on differential and dynamical measurements of gradients of gravitational potential, peculiar velocities, and matter density perturbations by methods of observational cosmology. There are also, however, direct astronomical methods of measuring the zeroth-order geometry bypassing the structure. For brevity, we will call them *geometrical*. These methods are advantageous at large scales because the Hubble flows build up with distance, while deviations from them decrease.

Geometrical tests deal with measurements of distances and times between events. In the zeroth order, these intervals are controlled by the function $a(t) \equiv (1+z)^{-1}$ and its derivatives. Both the properties of DE and other parameters of matter can be reconstructed by the measured cosmological functions $H(z)$ and $\gamma(z)$.

There are two classical astronomical methods of determining geometrical sizes: the measurement of radial distances or angular scales as functions of z . In the first case, we are dealing with the dependence ‘apparent magnitude-redshift’, $m = m(z)$, and in the second, the ‘angular size-redshift’, $\theta = \theta(z)$. Other geometrical tests exist, too (for example, counting the number of galaxies inside spheres of a given radius; see Fig. 2), but in this review we consider in more details only the two mentioned above.

The relationship $m = m(z)$ is called the Hubble diagram in astronomy. It allows determining the scale factor $a(t)$ of the Universe if the absolute luminosity is known for the objects being analyzed. Indeed, $(a^{-1} - 1)$ is the redshift of the source, and $(t_0 - t)$ is the distance to it in light years measured along the light cone of the past. Astronomers frequently use the *luminosity distance* r , which defines the flux \mathcal{F} of radiation from a point source of luminosity L_0 recorded on Earth, as if both the source and observer were in

the Euclidean space:

$$\mathcal{F} = \frac{L_0}{4\pi r^2}.$$

Instead of \mathcal{F} and L_0 , one may use the *apparent* m and *absolute* M stellar magnitudes, which are related to the distance r between the source and the observer as

$$m = M + 5 (\lg r [\text{pc}] - 1). \quad (45)$$

In order to estimate the absolute magnitude of the source luminosity, one needs to understand the source structure and the way it shine, i.e., to have a predictive theory. As a rule, this task is not solvable with the necessary accuracy, as we are dealing with a complex gasdynamic nonlinear system with many parameters, be it a galaxy or cluster of galaxies, a quasar, or a star. For this reason, one frequently resorts to empirical relationships that offer an estimate of object luminosity based on its other observable characteristics. These phenomenological relationships are built and validated on the nearest sources and then used to calibrate distant objects of the same class. It is implicitly assumed that near and distant sources of the same class are alike (the *standard candle* hypothesis).

While different objects have been proposed to play the role of the standard candle over years,¹⁰ this research cannot be used in rigorous cosmology as long as there is no theory for a system of that complexity, the theory based on numerical simulations and taking into account numerous, as yet little-studied, factors which pertain not only to the physical nature of objects (for example, star formation, nonstationarity, chemical composition, and nuclear fusion), but also to their environment, conditions of light propagation, and so on. For such data, a probability will always exist that we are dealing not with the effects of geometry or composition of the Universe, but rather with the internal properties of sources and their evolution (uncontrolled systematics).

While a standard candle is required for making use of Hubble diagrams, one needs to know the physical size of the observed object (the *standard rod* hypothesis) in order to measure distances by its angular size. Let the physical size of an object be d , and its angular size θ . The *distance based on*

¹⁰By way of example, the brightest cD galaxies in centers of rich clusters were used in the 1970-1980s as the standard candle. Currently, supernovae, gamma bursts, X-ray clusters of galaxies and other bright sources that yield to observations at large distances pretend on this role.

the angular size, D , is then defined as

$$D = \frac{d}{\theta}.$$

Making use of the interval of the Friedmann geometry, we get a relationship between the distances introduced above:

$$r = (1 + z)^2 D = (1 + z) R, \quad (46)$$

where R is the geodesic comoving distance to the object:

$$R \equiv \frac{\bar{R}}{H_0} = \eta_0 - \eta(z), \quad \bar{R} = H_0 \int_0^z \frac{dz}{H}. \quad (47)$$

(η is the conformal time). Apparently, the cosmological function $\bar{R}(z)$ depends only on the properties of matter, not on H_0 .

With the help of formula (46), any diagram $m(z)$ can formally be recast as the dependence $\theta(z)$, and vice versa. This is in no way surprising, as we are exploring *unified* geometry, even if resorting to various observational tests. In summary, the recipe for measuring the Universe is simple: construct diagrams $\theta(z)$ and $\dot{\theta}(z)$, or $m(z)$ and $\dot{m}(z)$, or others. If the physical size of the source or its absolute stellar magnitude are known, we will manage to determine the distance to it and, hence, the dimensions of the Universe. This will enable us to reconstruct the functions $H(z)$, $\gamma(z)$, along with other functions of the scale factor, and, in turn, determine the composition and properties of matter and their evolution with time.

The realization of this program requires highly accurate measurements and knowledge of the nature of the objects under study. In so doing, these objects can be very diverse. Figure 9 presents a cumulative diagram of $\theta(z)$ for several geometrical tests reduced to the standard size of $d = 9.5$ pc. Shown are the results of measuring distances based on the luminosity of distant Ia supernovae (points to the left of the minimum), the angular size of ultracompact radio sources (bases of jets from active galactic nuclei: six crosses in the lower part of the curve), and the anisotropy of CMBR (spectrum acoustic oscillations: the cross in the upper-right part). The dashed line corresponds to the CSM.

The most reliable point of observational data in this diagram is the right cross determined by the angular size of the acoustic horizon at the moment of recombination $z_{\text{rec}} = 1100$. The points and crosses found from observations of

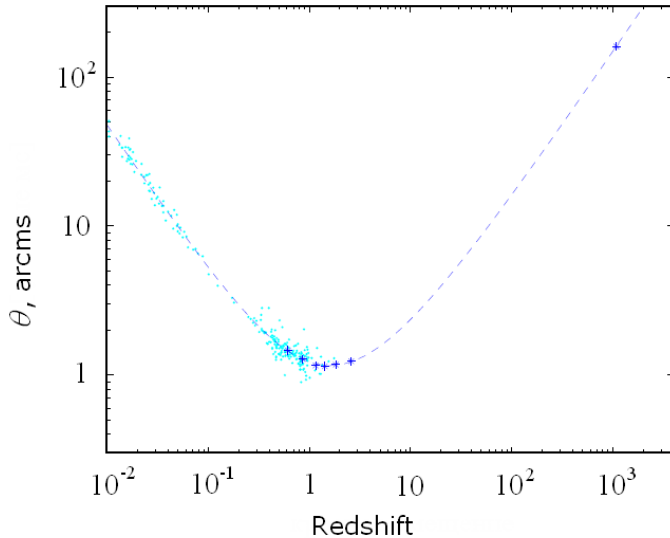


Figure 9: Diagram of $\theta(z)$ based on three geometrical tests reduced to the standard size $d = 9.5$ pc (according to Ref. [22]).

supernovae and ultracompact radio sources rely, respectively, on the standard candle and size hypotheses. There are certain physical grounds for using them. In the first case, we are dealing with the thermonuclear explosion of a binary white dwarf with total mass in excess of the Chandrasekhar limit setting the maximum luminosity of a supernova Ia. The second case pertains to the limiting mass of a central accreting black hole ($\sim 10^{10} M_{\odot}$, M_{\odot} is the mass of the Sun), which defines the ‘standard size’ of radio bright quasars. Note, however, that the available models of supernova explosions and active quasars do not meet for the moment the requirements placed on accurate geometrical measurements. Rather, the opposite approach can be beneficial: by knowing the answer (the parameters of CSM), we can inquire into the proper cosmological evolution and the nature of compact sources of that type.

Figure 10 demonstrates the image of an ultracompact radio source with minimum resolution on the order of a parsec, attained with the help of a terrestrial radiointerferometric network. The base of a jet can be seen well, but the internal structure of the source itself is unresolved. This example illustrates that exploration of compact objects, which lays the basis for di-

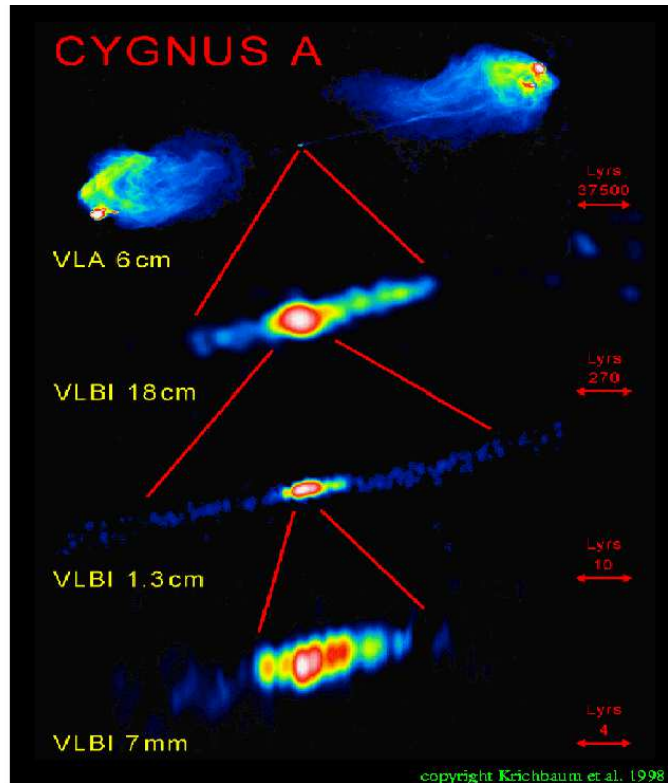


Figure 10: Ultracompact central radio source in Cygnus A (adapted from Ref. [23]). L_{yrs} is the distance expressed in light years.

rect geometrical measurements in the Universe, calls for the development of new techniques. Their realization is possible by making use of cosmic radio interferometry.

With the help of space telescopes, the interferometric baseline can be increased and, respectively, its resolution can be improved. Such instruments not only are capable of measuring distant compact objects but will also detect time *changes* in their angular sizes and redshifts, accompanying the expansion of the Universe. The last two factors are directly linked to the

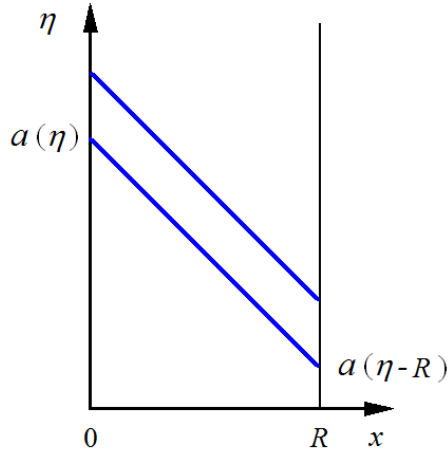


Figure 11: Trajectories of light rays in the Friedmann model in conformal coordinates (η, x) from the source $(x = R)$ to the observer $(x = 0)$ (see Ref. [2]).

Hubble function:¹¹

$$\frac{\dot{\theta}}{\theta} = -\frac{H(z)}{1+z}, \quad \frac{\dot{z}}{1+z} = H_0 - \frac{H(z)}{1+z}, \quad (48)$$

This opens new prospects for determining H_0 and $H(z)$ at cosmological distances.

Notice that if the DE density were constant, the redshift of the sources of the Hubble flow located at $z_0 \simeq 2.3$ would not change: $\dot{z}(z = z_0) = 0$. As this takes place, the redshift of more distant objects ($z > z_0$) decreases with time, and increases [$\dot{z}(z < z_0) > 0$] for less distant objects. The boundary $z = z_0$ is rather sensitive to the evolution of DE. Its detection will help answering the question of how the DE density varied in the past.

Determining the evolution effects (48) at cosmological distances will require several years of monitoring at angular resolution on the order of mi-

¹¹These relationships follow upon differentiating the functions

$$\theta = \frac{d}{R a(\eta - R)} \quad \text{and} \quad 1 + z = \frac{a(\eta)}{a(\eta - R)}$$

over η for constant d and R , where η is the observer time, and $(\eta - R)$ is the conformal time of the source (Fig. 11).

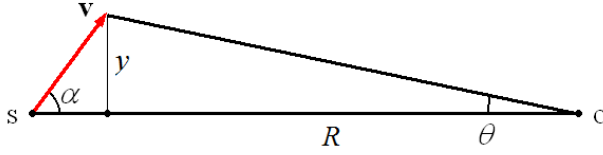


Figure 12: The plane (R, y) observer O and the jet node (the arrowhead) moving with velocity \mathbf{v} relative to the source S [2].

croarcseconds, which is technically challenging. However, even the first cosmic interferometers will be in a position to measure distances to nearby galaxies by their proper motion relative to the cosmic microwave background [18]. Moreover, one may measure distances by observing superluminal motion of the nodes of jets in active galactic nuclei, directed at a small angle to the line of sight. Such measurements are already being conducted on Earth (see, e.g., Ref. [24]) but can be essentially improved with the help of cosmic interferometers.

Let us clarify this effect in Fig. 12. Let α be a small angle between the motion direction of a jet node (the arrowhead) and the line connecting the observer O with the source S (quasar), and η and $\mathbf{x} = (R, y, 0)$ be the conformal coordinates of the node (R is the geodesic distance from the observer to the jet; see Eqn (47)). The observation time for the jet node moving with the intrinsic velocity \mathbf{v} is given by

$$d\tau = d\eta - dR = (1 - v \cos \alpha) d\eta,$$

and the apparent velocity of its displacement in the observer tangent plane is defined as

$$v_{\perp} = \frac{dy}{d\tau} = \frac{v \sin \alpha}{1 - v \cos \alpha} \leq v\Gamma. \quad (49)$$

This function passes through a maximum at $\cos \alpha = v$, equal to the jet gamma-factor $\Gamma \equiv (1 - v^2)^{-1/2}$ for the velocity $v = |\mathbf{v}|$ approaching the speed of light.

The jet displacement on the celestial sphere takes then the form

$$\dot{\theta}_{\perp} = \frac{v_{\perp}}{R} \leq \frac{0.3}{R} \left(\frac{\Gamma}{20} \right) \text{ arcms year}^{-1}, \quad (50)$$

which constitutes milliarcseconds per year for the superluminal velocities of bursts from quasars observed in reality (Fig. 13). By having extensive

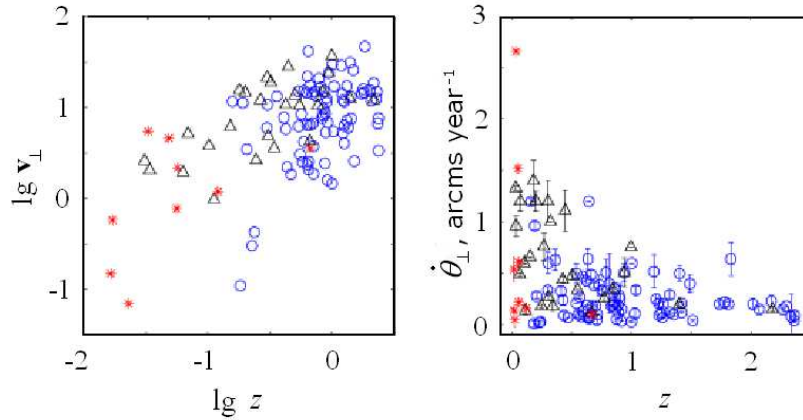


Figure 13: Superluminal ejections from quasars (see Ref. [25]): (a) the jet transverse velocity $v_{\perp}(z)$, and (b) angular displacement $\dot{\theta}_{\perp}(z)$.

statistics of such objects, we will be able to determine the geometrical characteristics $\bar{R}(z)$ (47) using the upper envelope of function (50).

We offered several examples illustrating the potential of direct assessment of geometry and composition of the Universe from observations of nonlinear objects. They can be augmented by observations of bright galaxies, compact groups of galaxies, rich X-ray clusters, gamma bursts, binary quasars, and other active systems. Exploring the Universe with their assistance remains not as efficient as that using quasilinear systems and based on measurements of large-scale structures, microwave background, and nonrelativistic matter. We may hope that the development of theory and numerical experiment will make the geometrical methods competitive in accurately solving the tasks of observational cosmology.

11 Formation of galaxies in the inhomogeneous Universe

How do the gravitationally bound halos of matter, reached hydrostatic equilibrium, emerge out of the quasi-Hubble flow¹² and how is the mass distribution of these nonlinear objects linked with the initial field of density perturbations?

In contrast to the large-scale structure bound up with relatively small matter density variations and staying at the beginning of its nonlinear development, the galaxies have evolved from high density peaks typical for the field of small-scale perturbations (less than several megaparsecs) and have already passed through the period of nonlinear relaxation. The reason for that is the amplitude and shape of the initial density perturbation spectrum which increases toward short wavelengths (see Ref. [1]). This property of spectrum facilitates early fragmentation of matter into ‘halo-blocks’ of small mass and their subsequent agglomeration in more massive halos of galaxies, groups, and clusters.

The hierarchical formation of nonlinear structures from small to large masses finds support in numerous observations and in numerical modeling. Important observational argument in favor of the sequential formation of halo systems is the absence of a large number of far emission Ly_α lines. The explanation is that massive systems, in their past, did not undergo a single powerful burst of star formation involving all halo gas, but formed by way of subsequent merges of numerous small-mass blocks that passed through their star formation phases at different times.

By virtue of the existing properties of the spatial S spectrum, the observable structure of the Universe possesses the following important features.

— The formation of galaxies and groups is largely completed, they contain the dominant part of DM. The process of galactic cluster formation still continues.

— Halos and their characteristics are distributed non-uniformly in space: their number and masses are modulated by the large-scale structure of the Universe.

— The first feature offers physical motivation for establishing a simple linkage between emerging nonlinear halos and peaks in linear seed density

¹²We also call the equilibrium halos relaxed or virialized systems, with the understanding that it is the virialization over velocities, not energies.

perturbations, based on the model of a quasispherical collapse [6]. The second feature invites us to apply the Press-Schechter method to finite-size domains and, in this way, to couple the mass function of halos with the large-scale structure of the Universe.

Before discussing theoretical predictions related to the halo mass functions and their validation against observations and numerical experiments, we remind the reader of the main characteristics and elements of the large-scale structure of the Universe. As we have already stressed, turning to large scales moves us to the initial stages of structure formation and the first phases of collapse, which are predominantly one-dimensional. Long-term observations of the spatial distribution of gravitationally bound virialized DM halos on scales of up to 300 Mpc demonstrate that the large-scale structure of the Universe possesses the following typical elements:

- *filaments* — linear structures of varying richness¹³ with lengths of up to tens of megaparsecs, and thickness of several megaparsecs;

- *walls* — flat formations reaching hundreds of megaparsecs over elongated directions and several megaparsecs in thickness, and filled with filaments;

- *nodes* — rich clusters of galaxies several megaparsecs in size occurring at intersections of filaments;

- *superclusters* — extensive domains of space from tens to hundreds of megaparsecs in size filled with walls, filaments, and nodes;

- *cosmological voids*¹⁴ — extensive domains reaching several hundred megaparsecs, where bright galaxies and galaxy clusters are absent.

The last two structural types are quasilinear because of their large size. Under the action of gravity, matter moves towards superclusters which expand more slowly than the mean Hubble flow. The matter ‘flows off’ the voids in different directions, and their local volume grows faster than the mean. The mean displacement of matter elements for the entire history of the Universe is smaller than the sizes of these structures and makes up 14 Mpc. The voids occupy the largest part of the Universe (more than 50%) and

¹³The richness of an element of a large-scale structure is defined by the number of galaxies composing it.

¹⁴The term cosmological ‘void’ reflects the fact that on celestial maps some regions seems to be empty. In reality, these cosmological empty domains can contain a significant (yet not dominant) fraction of the Universe’s matter, i.e., they are not really empty. That is why, instead of referring to cosmological ‘empty domains’, the term ‘voids’ is frequently used.

their forms in contours of low density are close to spherical, whereas superclusters are dense formations with a flattened shape. Both types of structures can naturally be characterized by the mean substance density within a given volume. It is smaller than the Universe's mean value in voids, and larger in superclusters.

Observational assessment of the parameters of voids and superclusters is ambiguous. The reason for the blurring of voids and superclusters reconstructed from the spatial light distribution resides in a nontrivial physical coupling between luminous matter and the DM composing the backbone of the structure. The resolution of these formations through the threshold density contrast of the matter contained in them compared to the mean level is more rigorous and accurate. We define voids (and superclusters) as three-dimensional spatial domains with a given negative (positive) level of matter density contrast. When the absolute value of threshold contrast decreases, the sizes of structures grow, and their number decreases. For $\rho < \rho_c$, we obtain a single void filling the whole Universe.

An important characteristic of voids and superclusters is the mass function of the halos populating them. Observations indicate that the cosmological voids nearest to us are impoverished in normal and dwarf galaxies, but weakly emitting galaxies and gaseous clouds are encountered. They are observed both through the ultraviolet absorption lines in the spectra of quasars or bright galaxies placed behind them and the absorption line of neutral hydrogen (21 cm) in the spectra of distant radio sources. Galaxies in voids are of reduced luminosity on average, compared to those in superclusters, though the slopes of their luminosity functions differ but slightly from each other [26].

The theory predicts that voids and superclusters contain weak galaxies of small mass that have not passed the stage of active stellar formation, as well as primordial objects of the hierarchical clustering model with masses up to $10^5 M_\odot$ and less. Such objects are incapable of holding gas, so that stellar formation in them is practically impossible. With growth in measurement sensitivity, observers are succeeding in finding previously unknown weak galaxies with masses of $10^7 - 10^9 M_\odot$ in the Local Group and the nearest neighborhood [14]. Their number agrees well with the predictions of the CSM, yet the question of finding lessmassive galaxies remains open to date.

The minimum cutoff scale for the spectrum of initial density perturbations is linked to the physics of DM and is still unknown. The region of small masses that yields to exploring by means of observational cosmology (for

example, by observing forest of absorption lines in the spectra of distant quasars) can be linked to the temperature T of the Universe at an instant of time when the comoving size R of a given mass M_R coincides with Hubble's radius of the Universe:

$$R \simeq 10 \left(\frac{10 \text{ keV}}{T} \right) \text{ kpc}, \quad M_R \simeq 10^5 \left(\frac{10 \text{ keV}}{T} \right)^3 M_\odot.$$

Numerical modeling of processes pertaining to the formation of structure from cold matter has led to substantial advances in exploring the mass functions of nonlinear halos in different domains of the Universe. Starting simulations of the formation process at $z \sim 20$ with seed masses $M \sim 10^5 M_\odot$, to $z \sim 0$ one manages to obtain a spatial distribution of gravitationally bound systems with typical masses in the range $\sim 10^{12} - 10^{13} M_\odot$ (see Refs [27] - [32]), which is similar to the distribution observed. In this case, all dark matter proves to be involved in the virialized halos of all sorts of masses, while the mean matter density inside the halos at the instant of their formation exceeds the mean density in the Universe by a factor of ~ 200 . This corresponds to the predictions of quasispherical collapse.

12 Mass function of relaxed halos

The Press-Schechter approximation relies on two assumptions.

(1) The linear perturbation field is Gaussian: the volume fraction of the Universe where the density contrast $\delta_R(z, \mathbf{x})$, smoothed over a sphere of radius R [see Eqns (61), (62)], exceeds a certain threshold value δ_c is given by

$$f(M, z) = \frac{1}{\sqrt{2\pi}} \int_\nu^\infty e^{-\nu'^2/2} d\nu', \quad (51)$$

where

$$\nu = \nu(M, z) \equiv \frac{\delta_c}{\sigma_R(z)} \quad (52)$$

is a monotonically increasing function of argument $M \equiv M_R = 4\pi\rho_m R^3/3$, and

$$\sigma_R(z) = \bar{g}(z) \cdot \sigma_R \quad (53)$$

is the variance of density contrast in a sphere of radius R (see Ref. [1] for more detail). The connection of the normalized factor of density perturbation

growth with those introduced earlier is defined as

$$\bar{g}(z) = \frac{g(a)}{g(1)} = \frac{\hat{g}(a)}{\hat{g}(1)}. \quad (54)$$

(2) The matter in density peaks collapses and stays confined in gravitationally bound objects: there is such a value δ_c whereat the mass fraction of matter in the Universe,¹⁵ $F(> M, z) = 2f(M, z)$, turns out to be involved in virialized halos with individual masses in excess of M by time moment z :

$$F(> M, z) = 2f(M, z) = \frac{1}{\rho_m} \int_M^\infty n dM. \quad (55)$$

where

$$n = n(M, z) \equiv \frac{\rho_m}{M} f_M \quad (56)$$

is the differential mass function (the mean number density of halos with masses M in the interval $dM \sim M$), and

$$f_M = f_M(z) = \left| \frac{d \ln \sigma_R}{d \ln M} \right| f(\nu) \quad (57)$$

is the fraction of matter that resides in halos with masses M by time moment z .

A comparison of expressions (51) and (55) allows us to determine the mean mass function of nonlinear halos in the Universe:

$$f(\nu) = f_{PS} \equiv \sqrt{\frac{2}{\pi}} \nu e^{-\nu^2/2}. \quad (58)$$

The normalization condition of the function f_M is written down as

$$\int_0^\infty f_M \frac{dM}{M} = 1 \quad (59)$$

¹⁵The numerical coefficient 2 implies that in the course of hierarchical clustering *all* the cold substance proves to be caught in virialized halos of all possible masses: $F(> 0, z) = 1$ for any z . The argument M is more convenient than R because M is preserved both for linear perturbations and for halo objects. If the component of massive neutrinos is included in the matter, we need to take into account the dependence of growth factor (53) on the spatial scale.

and it implies that for any z all the dark matter is confined in nonlinear halos. We can only inquire about the distribution of these halos over masses and about the typical halo objects for a given z , containing a dominant part of the Universe's matter. For large z , all the matter is decomposed into small masses, but the share of large halos grows with time. The mass of typical halos, M_* , at any epoch is defined by the condition

$$\nu(M_*, z) = 1.$$

For the modern Universe, one has $M_* \simeq 10^{13} M_\odot$. For small M , the function $f_M \sim \nu \ll 1$. This implies that halos of small mass are seized by more massive ones in the course of hierarchical clustering, i.e., they *leave* the set of M objects and are taken into account only in newly forming halos of larger mass.

The approximation of linear density contrast in the CSM at the instant of halo formation in the framework of homogeneous collapse¹⁶ gives the threshold contrast value $\delta_c = 1.675$, which only weakly depends on variations of cosmological parameters within their error bounds [33].

Long-term investigations have shown that the results obtained with the help of this method agree well with the numerical N -body experiment. Nevertheless, the basic formalism does not include mechanisms of merging and tidal breakup of objects. Hence, as a rule, the Press-Schechter method is applied to analyzing the spatial distribution of objects with a sufficiently high mass (such as clusters of galaxies), for which these effects are insignificant.

In order to apply this method in precise cosmology, account must be taken of corrections for the nonsphericity of collapse. Analytical estimates show how the function $f(\nu)$ is modified in this case. For constructing an accurate analytical approximation, we need to use a more general empirical formula enabling a nonspherical correction (the Sheth-Tormen approximation [34]):

$$f(\nu) = f_{ST} \equiv f_0 \sqrt{\frac{2}{\pi}} \tilde{\nu} (1 + \tilde{\nu}^{-p}) e^{-\tilde{\nu}^2/2}, \quad (60)$$

¹⁶In a simple cycloid model of a collapsing dust sphere $a = a_0 (1 - \cos(\sqrt{z}\eta))$, the time moment z of halo formation coincides with that of collapse, $t(z) = \int_0^a ad\eta = 2\pi a_0/\sqrt{z}$. Taking into account that the radius of a virialized halo is half that of the radius enclosing the same mass at the moment the cycloid stops, we conclude that the density of the halo at the instant of its formation exceeds that of a collapsing sphere at the instant of its stopping by a factor of 8. Hence, inter alia, a useful estimate follows for the halo radius at the halo formation instant – it is approximately six times smaller than the radius of a sphere enclosing the mass M in the unperturbed Universe. Speaking figuratively, a halo at its inception is a fragment of the unperturbed Universe compressed sixfold in scale.

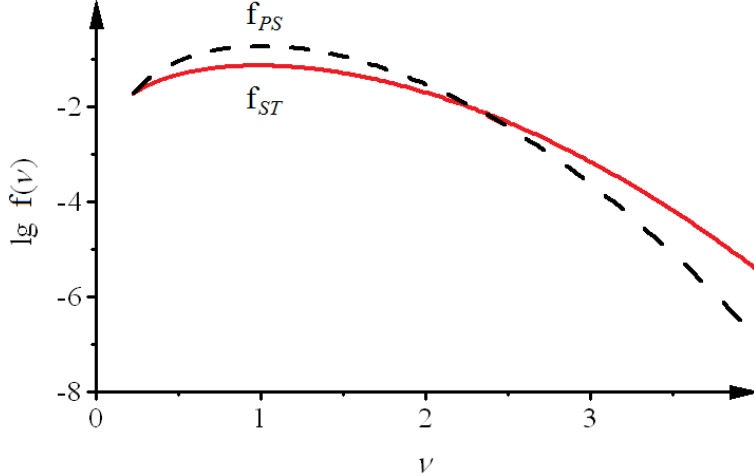


Figure 14: Functions $f(\nu)$ in the Press-Schechter (PS, dashed line) and Sheth-Tormen (ST, solid line) approximations of halo mass functions (see Ref. [2]).

where $\tilde{\nu} = \nu/\nu_0$, and find numerically the correction factors

$$f_0 = 0.32, \quad \nu_0 = 1.2, \quad p = 0.6$$

(f_0 is the normalization coefficient obtained from Eqn (59)).

Such a corrected approximation, accounting for the Gaussian perturbation field and the collapse of density peaks, ideally describes the results of numerical simulations and is widely used in modern cosmology (Fig. 14). Apparently, the Press-Schechter approximation somewhat over estimates the number of gravitationally bound halos with masses near the characteristic M_* ($\nu = 1$), but underestimates the number of massive halos with $M > 5 \times 10^{14} M_\odot$. The intersection of two functions happens at $\nu = 2.3$, which corresponds to the mass of order $\sim 10^{14} M_\odot$ in the current epoch (the precise value depends on the normalization of the spectrum; see Section 14).

In its standard form, the Press-Schechter formalism offers expressions only for the *mean* mass function of virialized halos, and misses such large-scale inhomogeneities as voids or superclusters, in which the local density ρ_L of matter on the scale L differs from the background one, ρ_m . In the next section we will obtain mass functions for halos populating the inhomogeneous Universe [35].

13 Modulation of galaxies by the large-scale structure

Local extended domains in the Universe can conveniently be characterized by the mean matter density inside a sphere of comoving radius L centered at a point \mathbf{r} :

$$\rho_L = \rho_L(\mathbf{r}, z) = \int \rho(\mathbf{r}', z) W_L(|\mathbf{r} - \mathbf{r}'|) d\mathbf{r}' \quad (61)$$

where

$$W_L(r) = \frac{3}{4\pi L^3} \begin{cases} 1, & r \leq L \\ 0, & r > L \end{cases} .$$

Let us introduce the parameters of mean density contrast and local matter density in the domain L :

$$\delta_L \equiv \frac{\rho_L}{\rho_m} - 1, \quad \Omega_L \equiv \Omega_m \frac{\rho_L}{\rho_m} . \quad (62)$$

Adding up expression (62) with Ω_E , we obtain the mean density of matter in the domain L . Subtracting from it the equality $\Omega_m + \Omega_E = 1$ for a flat Universe, we obtain the parameter Δ_L characterizing the mean curvature of domain L :

$$\Delta_L \equiv \Omega_L - \Omega_m \equiv \Omega_m \delta_L . \quad (63)$$

Distinct from R , the free parameter L is assumed to exceed the inhomogeneity scale ($L > 10$ Mpc), so that spatial domains with $\rho_L < \rho_m$ (voids ‘v’, Fig. 15) and $\rho_L > \rho_m$ (superclusters ‘s’) are still in the phase of quasi-Hubble expansion ($|\delta_L| < 1$). As $L \rightarrow \infty$, ρ_L tends to the mean matter density in the Universe, $\rho_m = \rho_m(z)$.

In order to construct the local halo mass function we should:

— resolve the field of linear perturbations of the density contrast δ_R into a large-scale background δ_L and a small-scale part $\delta_{R|L}$ which characterizes the seed perturbations leading to halo formation in a given spatial domain of size $L > R$ (see Fig. 15):

$$\delta_R = \delta_L + \delta_{R|L} , \quad (64)$$

— describe a quasispherical collapse on the background ρ_L instead of the homogeneous background of density ρ_m .

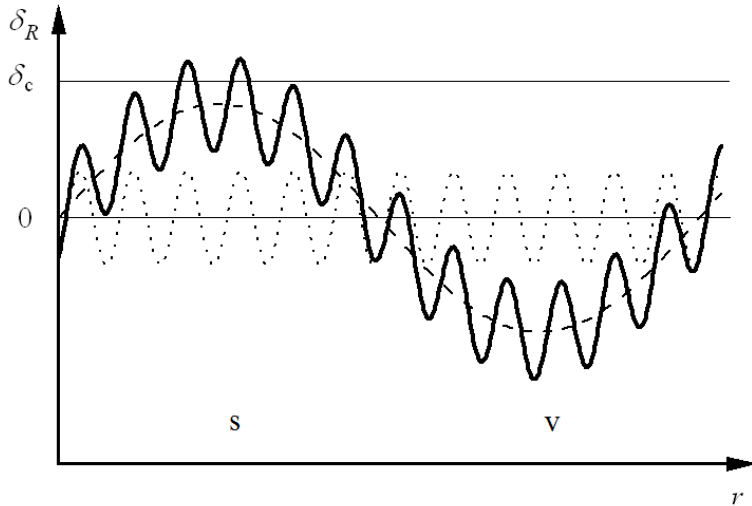


Figure 15: Spatial field of density contrast $\delta_R(\mathbf{r})$ (solid line) as the sum of long-wave background δ_L (dashed line) and short-wave residual $\delta_{R|L}$ (dotted line) [35]; δ_c is the threshold contrast.

From a physical viewpoint, we are considering the influence of the local large-scale structure of the Universe on the local process of hierarchical clustering. Assuming the scale of the structure is large ($L > R$), its influence on the collapse can be represented in the form of a power series in spherical harmonics. The monopole term in this series is the main factor influencing the local statistics of virialized halos, which lays the basis of this method. The dynamics of collapse depend only on the mass of the substance confined within a sphere of radius R ; however, the regions where the density contrast exceeds the threshold one are less abundant in voids than in superclusters. Namely this information is contained in the background offsetting the Gaussian function $\delta_{R|L}$. At this stage, we ignore the dipole (density gradient), quadrupole (tidal forces), and other terms in the structure expansion, which are linked to the motion of the halo as a whole and the nonsphericity of collapse. Their influence can be accounted for as numerical corrections to the halo mass function [see Eqn (60)].

The dispersion $\delta_{R|L}$ of a linear Gaussian field describing the local proper-

ties of density perturbations for $R < L$ takes the form¹⁷

$$\sigma_{R|L}^2 = \int_0^\infty P(k) |W(kR) - W(kL)|^2 k^2 dk. \quad (65)$$

Apparently, $\sigma_{R|L} \rightarrow 0$ for $M \equiv M_R \rightarrow M_L$ (the mass in the sphere of radius L).

Carrying out computations similar to those in Section 12, we obtain the halo mass function $M \in (0, M_L)$ in the domain L [35]:

$$n_L = n_L(M) \equiv \frac{\rho_L}{M} f_{M|L}, \quad (66)$$

$$f_{M|L} = \left| \frac{\partial \ln \sigma_{R|L}}{\partial \ln M} \right| f(\nu_L), \quad \int_0^{M_L} f_{M|L} \frac{dM}{M} = 1,$$

where the function $f(\nu)$ coincides with Eqn (58) (or Eqn (60) in the case of correction for nonsphericity), and ν_L follows from Eqn (52), with σ_R replaced by $\sigma_{R|L}$, and δ_c by $\delta_{c|L}$.

The function $\nu_L = \nu_L(M, z)$ grows monotonically with the mass growth and diverges when $M \rightarrow M_L$. The threshold density contrast $\delta_{c|L}$ depends on the local density of background. When computing $\delta_{c|L}$ it should be borne in mind that the domains of superclusters with $\delta_L > 0$ (or voids with $\delta_L < 0$) expand more slowly (faster) than the homogeneous background. A smaller (larger) threshold contrast $\delta_{c|L}$ with respect to the actual background will assure the collapse of a given domain of increased density up to a time moment z :

$$\delta_{c|L} = \delta_c - \delta_L. \quad (67)$$

This formula is valid in the linear order in δ_L . Numerical correction is needed to account for nonlinear contributions.

Figure 16 presents halo mass functions Mn_L/ρ_m at $z = 0$ in a void, supercluster, and flat domain of space with dimensions $L = 140$ Mpc and different values of mean density contrast δ_L . As can be seen, *small-mass* halos form the main population of zones with a reduced matter density.

For example, the fractions of substance in a void with $\delta_L = -1/2$, existing in the form of primary isolated blocks – halos with masses $10^7 M_\odot$, $10^9 M_\odot$,

¹⁷Here, the field crosscorrelation between $\delta_{R|L}$ and δ_L is neglected. It is significant only at $R \sim L$.

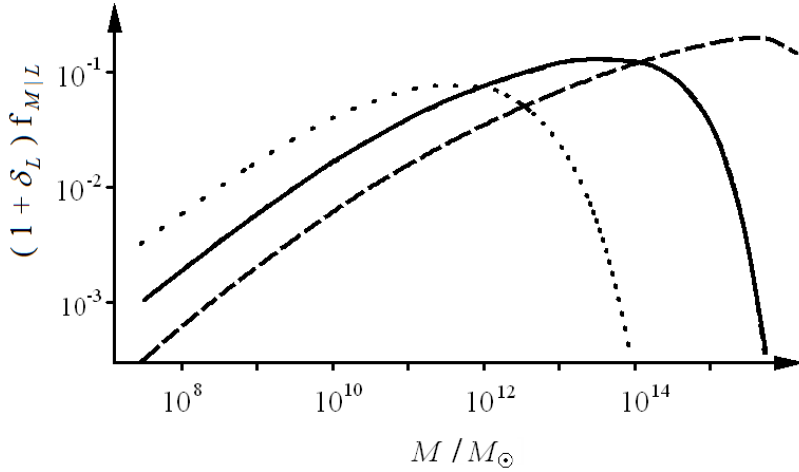


Figure 16: The DM fraction $(1 + \delta_L) f_{M|L}$ in the halo of masses M (in the interval $\delta M = M$) in the domains of the modern Universe with the size of $L = 140$ Mpc and density contrast δ_L (see Ref. [35]). The curves correspond to a supercluster (dashed, $\delta_L = 1/2$), flat background (solid, $\delta_L = 0$), and void (dotted, $\delta_L = -1/2$).

and $10^{11} M_\odot$ – constitute about 1, 10, and 30%, respectively. It is easier, therefore, to discover low-mass primary objects of DM, which are not confined in more massive halo systems, in voids than in other parts of the Universe.

The solid line for spatially flat domains of the CSM in Fig. 16 characterizes the modern Universe as a whole. We see that the range $5 \cdot 10^{11} - 5 \cdot 10^{13} M_\odot$ of halo masses (massive galaxies and groups of galaxies) hosts 30% of the total DM in the Universe, and massive halos with $M > 5 \times 10^{14} M_\odot$ (rich clusters of galaxies) include no more than 10% of its nonrelativistic matter ($f_M < 0.1$).

Thus, the process of hierarchical gravitational clustering, collecting the dominant part of low-mass objects into more massive systems with $M \lesssim 5 \cdot 10^{13} M_\odot$ and observed as a phase of the active merging of galaxies, is completed in the Universe on the whole. For more massive formations with $M \gtrsim 10^{14} M_\odot$ this process, seen as the interaction of groups and clusters, still continues and is far from completion.¹⁸

¹⁸The patchy structure of most galaxy clusters in X-ray spectral region offers an addi-

If we consider separate domains of space, the coalescence of galaxies and interaction of galaxies there followed their own ways in the past and continue to do so. Indeed, clustering of halos in voids fully ceases with time [see the limit mass M_L in Eqns (65) and (66)]. In contrast, in ‘flat’ zones and in regions of augmented density, the clustering and coalescence are progressing and gradually shift toward larger masses. We may argue that the activity in the form of coalescences, accompanying the process of galaxy formation everywhere in the Universe since its beginning, degenerates with time, continuing in flattened superclusters and breaking down in voids. The process resembles a burning out fire.

As a result, the morphology of galaxies proves to be different at various locations in the Universe. Notably, finding *isolated galaxies* which lack adjacent partners of comparable mass is, for instance, more probable in voids and close to their boundaries than in superclusters. In contrast, interacting galaxies are more common in superclusters, beginning with pairs and ending with large associations or clusters.

Summarizing, we can conjecture that the theory considering the formation of the nonlinear structure from DM agrees well with observations and numerical experiments and has a predictive skill valuable for further research. There still remain some problems related to the evolution of the baryon component. Solving them hinges on further development of computer facilities, observational techniques, and data processing methods.

The halo mass functions in voids and superclusters differ substantially. In particular, the spatial density of massive ($M \sim 10^{12} M_\odot$) halos in voids is several times less than in superclusters, and the distinction in mass functions is even larger for larger masses. In regions of galaxy clustering, the observational statistics worsen:

$$n(M) \simeq 2 \cdot 10^{-5} \exp\left(-\frac{M}{M^*}\right) \text{Mpc}^{-3}, \quad (68)$$

where $M^* \simeq 4 \cdot 10^{14} M_\odot$ on the average in the Universe. For this reason, the comparison of theory against experiment relies on *integral* functions of halo masses, possessing more extensive data statistics.

The integral mass function describes the full number of halos N_L in the

tional argument in favor of this statement.

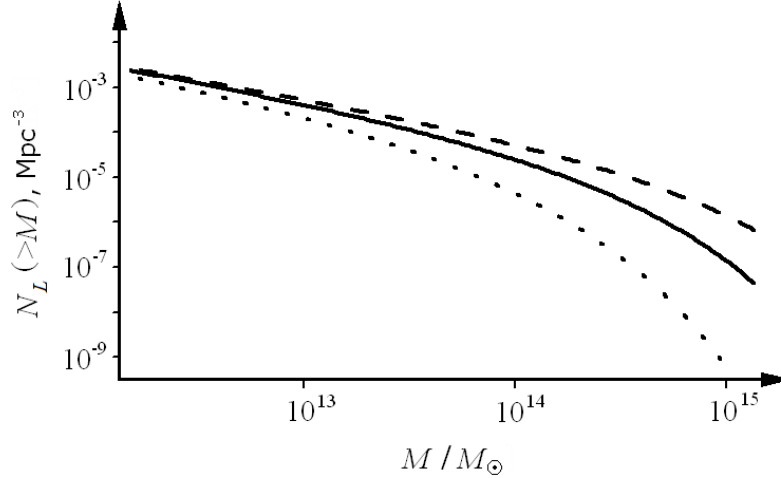


Figure 17: Integral mass functions $N_L(> M)$ of equilibrium halos in the range $10^{12} - 10^{15} M_\odot$ for the same domains of the Universe as in Fig. 16.

domain L (reduced to a unit volume) with masses in excess of a given one:

$$N_L(> M) = \int_M^{M_L} n_L(M) \frac{dM}{M}. \quad (69)$$

The differences between the integral functions in voids and superclusters diverge exponentially with increasing M , because the characteristic values M_L^* of halo masses are different there (Fig. 17). In the region of small masses (dwarf galaxies), the integral functions are hardly distinguishable, and the $f_{M|L}$ functions appear more appropriate (see Fig. 16). The actual distinction between mass populations of voids and superclusters is stronger because of the nonlinear galaxy coalescence effects and tidal destruction of galaxies, which partly suppress the small-mass part of the mass function in superclusters.

The main population of voids is *primordial objects* (POs) with small masses. The share of the matter in voids in the form of isolated galaxies with $M < 10^9 M_\odot$ reaches 10%, whereas it does not exceed 1-2% in other domains of the Universe. Globular clusters in the central regions of massive galaxies can be stellar remnants of POs: they could have formed in molecu-

lar clouds of the first small-mass halos and then accumulated in the central regions of massive galaxies in the process of hierarchical clustering.

The primordial objects in voids can manifest themselves as weak dwarf galaxies or in the form of Ly_α absorption systems. Indeed, we can estimate their spatial density and dimension, assuming that their formation epoch $z_0 \sim 10$ and mean mass $M \sim 10^7 M_\odot$, as

$$n_{\text{PO}} \sim \frac{\rho_m}{M} \sim 10^4 \text{ Mpc}^{-3}, \quad r_{\text{PO}} \sim \frac{1}{6} n_{\text{PO}}^{-1/3} (1 + z_0)^{-1} \sim 1 \text{ kpc}.$$

As can be seen, these primary formations are rather loose, so that lensing effects on them are unimportant. The possibility of discovering them depends on their subsequent evolution. One may hope that such objects have retained their gaseous component in voids and that their column hydrogen density appears sufficient for the emergence of weak Ly_α absorption lines. The probability of picking such objects up in the line of sight in a void of size $L \sim 100 \text{ Mpc}$ is on the order of unity: $n_{\text{PO}} r_{\text{PO}}^2 L \sim 1$.

14 Normalization of scalar perturbations

Data on the anisotropy of the CMBR give exact information on the amplitude and shape of the initial S spectrum in the *early* Universe and on certain parameters of composition (densities of nonrelativistic components, and the curvature of space). However, to trace the transformation of initial inhomogeneities into the observed galaxies, we also need to know the growth factor for density perturbations in the *late* Universe, which depends on the Hubble radius and DE (see Sections 6 and 7). The number and mass distribution of gravitationally bound relaxed halos, formed through the development of the gravitational instability of DM, depend *exponentially* on the amplitude of initial scalar inhomogeneities in the curvature and growth factor of density perturbations (see Sections 12 and 13). Owing to this dependence, we have at our disposal a sensitive test enabling us to determine the amplitude and shape of the S spectrum together with the most important supplementary parameters of the Universe's composition from the quantitative characteristics of the structure.

This test is frequently referred to as the normalization of the spectrum of cosmological density perturbations. For a given observed mass distribution of gravitationally bound DM halos, the amplitude of the power spectrum

is a function of cosmological parameters (Ω_m , Ω_E , and others) within their variability bounds admitted by the data accuracy.

For historical reasons, the normalization ‘to sigma 8’ – the dispersion of density contrast within a sphere of radius $8h^{-1}$ (in this section, $h = H_0/100 \text{ km s}^{-1} \text{ Mpc}^{-1}$), which represents the integral function of the density perturbation spectrum – is used most widely. We denote this dispersion as σ_{11} here to emphasize its actual value: $8h^{-1} \simeq 11 \text{ Mpc}$. The sphere encloses the mass of an unperturbed Universe, $M_{11} \simeq 2 \cdot 10^{14} M_\odot$, which is close to that of a typical cluster of galaxies. This normalization test is therefore ideally oriented to using observational data on the abundance of galactic clusters. Moreover, the theoretical analysis of halo mass functions in this mass range relies on an elaborate analytical formalism (see Sections 12, 13).

The magnitude of dispersion σ_{11} , which ensures the observed spatial number density of clusters, essentially depends on the total matter density Ω_m in the Universe, whereas changes in all other cosmological parameters affect σ_{11} only within 10-20% of its magnitude. We will demonstrate below the technique of normalizing the density perturbation spectrum to the abundance of galaxy clusters at $z = 0$, which satisfies the current requirements of precise cosmology [36].

All cosmological parameters can be spread between two levels according to their impact on the quantity σ_{11} :

- Ω_m (the first level);
- Ω_E , h , n , f_ν , Ω_b , w_E , and others (the second level), where $f_\nu \equiv \Omega_\nu/\Omega_m$ is the fraction of matter in the form of massive neutrinos. Among the free parameters of the second level, the first four are statistically significant (within intervals of their variability). The rest are fixed for simplicity ($\Omega_b h^2 = 0.023$, and $w_E = -1$).

A class of models to be utilized represents a rather advanced variant of the CSM extension at the modern knowledge level: it includes the nonzero spatial curvature ($\Omega_\kappa = 1 - \Omega_m - \Omega_E$), hot, cold, and baryonic components of matter ($\Omega_m = \Omega_\nu + \Omega_M + \Omega_b$), the cosmological constant, and nonflat (but power-law with the slope n) spectra of the S mode. In this class of models, the exact dependence of the threshold density contrast δ_c on Ω_m and Ω_E in the curved Universe is also taken into account [33].

The subsequent study is split into two stages. At the first stage, an optimum value of σ_{11} with accompanying individual error was computed through the comparison of theoretical and observational differential functions of cluster masses for every realization of the extended model (with its own

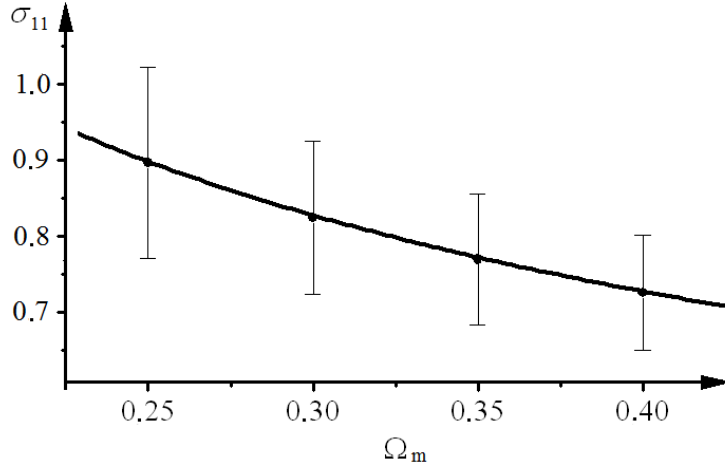


Figure 18: The dispersion $\sigma_{11}(\Omega_m)$ of density contrast in a sphere of 11 Mpc in radius for the CSM [36]. The vertical lines show the accuracy of observational optical data on the abundance of near clusters of galaxies (a confidence level of 95%).

set of cosmological parameters).¹⁹

At the second stage, all the computed values of σ_{11} (they are tens of thousands in number, and each has its own error) were fitted by the approximating dependence of the form [36]

$$\sigma_{11} = \Omega_m^{A_1+A_2} \Omega_m^{A_3} \Omega_E [A_4 + \quad (70)$$

$$+ A_5 (\Omega_m - A_6) (1 - A_7 h - A_8 n - A_9 f_\nu)],$$

The optimal values of parameters A_i ($i = 1, 2, \dots, 9$) were determined by the Levenberg-Marquardt method of χ^2 minimization. Notice the important distinction of this stage from the previous one. In the first case, $n(M)$ was a function of a single variable (mass M). In the second case, the function σ_{11} depended on multiple variables (Ω_m , Ω_E , h , n , and f_ν).

¹⁹The approach presented here can work with arbitrary observational data pertaining to virial masses of galaxy clusters. In the particular case considered here the results of optical observations of the speeds of galaxies in the nearest 150 clusters with a median value of redshift $z \simeq 0.05$ (see Refs [37, 38]) were utilized.

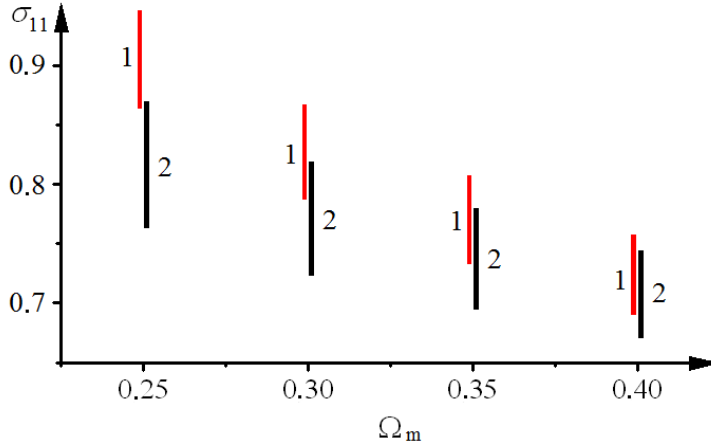


Figure 19: Projection of the space of cosmological parameters in the extended CSM onto the plane (σ_{11}, Ω_m) for the Sheth-Tormen (bars labeled with 1) and Press-Schechter (labeled with 2) approximations (from Ref. [36]).

Figure 18 illustrates the second phase of normalization. It shows the slice of the cosmological parameter space of the extended model in the two-dimensional plane of main parameters (σ_{11}, Ω_m) . In this case, the standard values were taken for other cosmological parameters ($\Omega_E = 1 - \Omega_m = h = 0.7$, $n = 1$, $f_\nu = 0$). The plot confirms the expected, strong dependence of σ_{11} on Ω_m .

The experience of working with different data indicates that the value obtained for σ_{11} depends on the selection of observations. We have already mentioned that this is, unfortunately, a common story accompanying work with nonlinear objects (clusters of galaxies in this case). This should be borne in mind when mentioning the ‘standard values’ of, first of all, such parameters as σ_{11} , H_0 , and Ω_m (or Ω_E). They, to a larger degree than any other quantities, depend on observations of astronomical objects (stars, quasars, galaxies, and clusters). There is only one way out: improvement in the quality of observational data and control of systematic effects related to the evolution of the baryonic matter component.

We now turn to other parameters. The fact that their contribution to σ_{11} is statistically significant is vividly illustrated, besides by formulas [see Eqn (71) below], by Fig. 19. All the space of models is projected there onto the

plane (σ_{11} , Ω_m). As can be seen, the height of bars σ_{11} for various values of parameters Ω_m , h , n , and f_ν is comparable to the size of statistical error, and exceeds it for some sets of cosmological parameters. This emphasizes the importance of a thorough account of the contributions from all model parameters mentioned above.

An interesting result, also seen from Fig. 19, is the increasing influence of the second-level parameters as the values of Ω_m reduce. Since the interest of modern cosmology is focused namely on this domain, this once again confirms the necessity of simultaneous account of all cosmological parameters when solving cosmological tasks at a high level of accuracy. The scatter of σ_{11} upon variations of second-level parameters looks tighter for the Sheth-Tormen approximation, which says something about its advantage: it ensures the most accurate power spectrum normalization in work with mass functions of galaxy clusters (see, for instance, Ref. [39]).

We specify the form of formula (70) for the normalization of the scalar perturbation spectrum as obtained in Ref. [36], which compared the abundance of optical galaxy clusters with the theoretical halo mass function derived in the Sheth-Tormen approximation in the extended CSM:

$$\sigma_{11} \Omega_m^{0.54 + 0.15 \Omega_m - 0.04 \Omega_E} = \dots \quad (71)$$

$$-0.2 (\Omega_m - 0.75) (1 - 0.2 h - 0.2 n + 0.8 f_\nu) = 0.53 \pm 0.08.$$

Here, the left-hand side contains combinations of cosmological parameters, whereas all errors are mapped into the right-hand side and attributed to the normalization (a confidence level of 95%).

This example illustrates the specifics of cosmological research with respect to observational data:

- the need for *multidimensional* spaces of parameters to determine the main model characteristics,
- the need for *numerous* multivariate observational tests to lift the problem of parameter degeneration.

As follows from the example above, formula (71) alone is insufficient to normalize the S spectrum amplitude itself: we only know the relationship between the parameters, and need additional data to solve the normalization task. Note also an interesting feature of this formula: it has the form of a ‘plane’ for the second-level parameters. The coefficients of this plane may be refined by more complete data of future observations.

15 Conclusions

Summing up, we can argue that the standard theory for the structure formation in the Universe in the framework of the CSM does not encounter principal problems in explaining the observed matter motions and distributions. The theory of nonlinear structure formation hinges on the dominance of DM. It agrees well with observations and numerical experiments and has predictive skills for further research. There remain complex problems pertaining to the nonlinear dynamics of DM and the evolution of the baryonic component (we consider some of them in Ref. [1]). Solving the problems listed above and those related to them will benefit from the development of computer facilities, new methods of observation and data processing, and the refinement of cosmological parameters aimed at further improvement of the theory and extension of the CSM.

Acknowledgments.

The authors are indebted to S V Pilipenko for the fruitful discussions. The work was carried out with the support of RFBR grants OFI 09-02-12163, 11-02-00857, and FTsP ‘Scientific and scientific-pedagogical personnel of innovative Russia’ for 2009-2013 (State contracts P1336 and 16.740.11.0460). A M M is indebted to the Educational-Scientific complex of FIAN and the Special Program of the RAS Presidium in support of young scientists.

16 Appendices

A. Quasi-Hubble flows in the GRT

Appendices A, B, and C present the main features of inhomogeneous cosmological models in which the Friedmann symmetry is fully broken, yet the departure from it remains small [2]. Such models, deviating only slightly from the spatially flat Friedmann model, are called here *weakly inhomogeneous* or *quasi-Friedmann*, the flows spawning them, quasi-Hubble, and the geometrical departures proper, considered in the linear order of smallness, cosmological *perturbations*.

One of the most important geometrical characteristics in the GRT is the Einstein tensor, or the stress-energy tensor of matter T_{μ}^{ν} . Energy and momentum are carried in spacetime along timelike world lines – flow trajectories.

A vector tangent to them, u^μ , is the eigenvector of tensor T_μ^ν :

$$T_\mu^\nu u^\mu = \varepsilon u^\nu, \quad (72)$$

and its eigenvalue $\varepsilon = \rho c^2$ is the scalar of total comoving density.²⁰ The unit vector u^μ ($u_\mu u^\mu = 1$) describes the transport velocity of total flow energy. By definition, one has

$$p_{\alpha\nu} u^\mu T_\mu^\nu = 0,$$

where $p_\mu^\nu \equiv \delta_\mu^\nu - u_\mu u^\nu$ is the projective tensor orthogonal to u^μ . Accordingly, the symmetric tensor $p_{\alpha\nu} T_\beta^\nu$ describes the pressure structure.

In the Friedmann Universe, solution (72) is unique for all forms of matter: the components of a medium move along the vector u^μ (in Friedmann's coordinates $u^\mu = \delta_0^\mu$). The stress-energy tensor of matter has a universal form which contains the only 'new' scalar $p = p(t)$, the effective pressure in the medium:

$$T_\mu^\nu = (\varepsilon + p) u_\mu u^\nu - p \delta_\mu^\nu = \varepsilon u_\mu u^\nu - p p_\mu^\nu. \quad (73)$$

For weak perturbations of the Friedmann group, different medium components move in different directions, but deviations of their velocities from the mean velocity u^μ are small. Under this condition, solution (72) is unique and we obtain the general form of T_μ^ν in the quasi-Friedmann geometry:

$$T_\mu^\nu = (\varepsilon + p) u_\mu u^\nu - p \delta_\mu^\nu - s_\mu^\nu = \varepsilon u_\mu u^\nu - (p p_\mu^\nu + s_\mu^\nu), \quad (74)$$

which contains, in addition to the form (73), a small stress tensor s_μ^ν orthogonal to the flow u^μ ($u^\mu s_\mu^\nu = 0$). As we see, the total tensor of quasi-Hubble flow pressure comprises two terms: the diagonal tensor p , and the anisotropic stress tensor s_μ^ν . The total pressure can be determined by the trace of the pressure tensor:

$$p_{\text{tot}} = \frac{1}{3} p^{\mu\nu} T_{\mu\nu} = p + \frac{1}{3} s_\nu^\nu. \quad (75)$$

In a weakly inhomogeneous model, as in the Friedmann model, the rules of linear superposition are valid for matter components interacting only gravitationally:

$$\varepsilon = \Sigma \varepsilon_m, \quad p = \Sigma p_m, \quad u^\mu = \Sigma f_m u_m^\mu, \quad (76)$$

²⁰In the energy units of measurement adopted by us, energy and mass densities coincide ($c = 1$). Their different notations ε and ρ , respectively, are only important for dimensionality recovery and passages to the limit. For example, $G\rho$ does not contain the physical constant – speed of light in vacuum – and possesses the same dimensionality as H^2 .

where scalars f_m of partial contributions of matter components have the form

$$f_m \equiv \frac{\varepsilon_m + p_m}{\varepsilon + p}, \quad \Sigma f_m = 1, \quad m = 1, 2, \dots, M.$$

For general nonlinear interactions, the resolution of densities and pressures into components is ambiguous; however, notions of partial enthalpies $W_m \equiv \varepsilon_m + p_m$ and component velocities u_m^μ , as well as total ε and p , are preserved. Notice that these simple linear superpositions of medium component velocities are valid for terms of zeroth and first orders of smallness with respect to deviations of velocities u_m^μ from the mean one u^μ .

Projecting the Bianchi identities $T_{\mu;\nu}^\nu = 0$ onto u^μ and orthogonal directions, we arrive at equations for the energy and momentum of the total flow:

$$u^\nu \varepsilon_{;\nu} + 3H_\nu (\varepsilon + p_{\text{tot}}) = 0, \quad (77)$$

$$a_\mu \equiv u^\nu u_{\mu;\nu} = u^\nu (u_{\mu;\nu} - u_{\nu;\mu}) = \frac{p_{\mu;\nu}^\nu}{\varepsilon + p}, \quad (78)$$

where $H_\nu = u^\nu_{;\nu}/3$ is the Hubble factor of medium local *volume* expansion, and a_μ is the flow acceleration ($a_\nu u^\nu = 0$). To make the resolution of pressure into isotropic and anisotropic parts unique, we demand that the scalar part of s_μ^ν be of zero divergence [see Eqn (81)].

In the class of *quasi-Friedmann* coordinate splits (t, \mathbf{x}) , where the three-dimensional flow velocity is always small (D and v are small functions):

$$u_\mu = (1 + D, v_{,i}), \quad (79)$$

the decomposition of geometrical variables into the background and perturbation parts yields

$$g_{\mu\nu} = g_{\mu\nu}^{(F)} + h_{\mu\nu}, \quad (80)$$

$$g_{\mu\nu}^{(F)} = \text{diag} (0, -a^2 \delta_{ij}), \quad \frac{1}{2} h_{\mu\nu} = \begin{pmatrix} D & C_{,i}/2 \\ \text{sym} & a^2 (A \delta_{ij} + B_{,ij}) \end{pmatrix},$$

$$\varepsilon = \varepsilon^{(F)} + \delta\varepsilon, \quad p = p^{(F)} + \delta p, \quad (81)$$

$$s_\mu^\nu = \text{diag} \left(0, \frac{\Delta S \delta_{ij} - S_{,ij}}{8\pi G a^2} \right), \quad s_{\mu,\nu}^\nu = 0,$$

where sym denotes a symmetric matrix, and the letter F (discarded below when possible) labels the Friedmann variables. They are functions of t and obey the equations

$$\frac{3}{2}H^2 = 4\pi G\varepsilon^{(F)}, \quad \dot{\varepsilon}^{(F)} + 3H(\varepsilon^{(F)} + p^{(F)}) = 0. \quad (82)$$

The scalar sector of perturbations is fully described by four gravitational (A, B, C, D) and four material potentials ($v, \delta\varepsilon, \delta p$, and S for arbitrary physical fields!). The scalar S of anisotropic pressure is gauge invariant, while the remaining seven functions are not.²¹

The gauge invariant variables for the dimensionless velocity potential and perturbations of density and pressure in the matter have the form

$$q = A + H v, \quad \delta \equiv \frac{\delta\varepsilon_c}{\varepsilon + p}, \quad \delta_p \equiv \frac{\delta p_c}{\varepsilon + p}. \quad (83)$$

where the Lagrangian variables are

$$\delta\varepsilon_c \equiv \delta\varepsilon - \dot{\varepsilon} v = \varepsilon - \varepsilon_c, \quad (84)$$

$$\delta p_c \equiv \delta p - \dot{p} v = p - p_c = p_{\text{tot}} - p_v. \quad (85)$$

The scalar of a volume pressure $p_v = p_c + s_\nu^\nu/3$ and background functions $X_c \equiv X^F(t_c)$ describe distributions on spacelike hypersurfaces of constant *comoving* time $t_c = t + v$.

The field $q = q(t, \mathbf{x})$ plays a central role in the description of density perturbations [10, 11]. It has a double physical sense: on the one hand, it

²¹It should be reminded that the vortex and tensor parts of s_μ^ν are linked with V and T perturbation modes and are not considered here. Decompositions (80) and (81) of geometrical objects into a background and perturbations are not unique: under a small coordinate transformation $x^\mu \rightarrow x^\mu - \xi^\mu$ we will obtain a new background (the same background functions, but for other time t) and new perturbations, but the total geometry will be preserved. Expanding a small arbitrary vector $\xi_\mu = (X, a^2 Y_{,i})$ in two potentials X and Y , we get the following gauge transformations for scalar variables:

$$\begin{aligned} h_{\mu\nu} &\rightarrow h_{\mu\nu} + \xi_{\mu;\nu} + \xi_{\nu;\mu}, & u_\mu &\rightarrow u_\mu + X_{,\mu}, \\ A &\rightarrow A - HX, & B &\rightarrow B + Y, & C &\rightarrow C + X + a^2 \dot{Y}, \\ D &\rightarrow D + \dot{X}, & v &\rightarrow v + X, & t &\rightarrow t - X. \end{aligned}$$

is the dimensionless potential of the total matter velocity (laboratory interpretation), while, on the other hand, it is the potential of spatial curvature (cosmological interpretation). From the Einstein equations in the lowest order one derives the relationship between the potentials of the S mode and the field q :

$$\frac{\Delta\Phi}{a^2} = 4\pi G \delta\varepsilon_c, \quad \Phi = \frac{H}{a} \int (\gamma q - S) \frac{da}{H}, \quad (86)$$

$$v - C + a^2 \dot{B} = \frac{\mathbf{q}}{H}, \quad \dot{v} - D = \frac{\dot{q}}{H}, \quad (87)$$

$$\delta_p = \frac{\dot{q}}{H}, \quad (88)$$

where $\mathbf{q} \equiv q - \Phi$ is the potential of the peculiar velocity of matter [see Eqn (101) below]. Hence, notably, having chosen $v = C = 0$, we obtain the metrics in the Lagrangian orthogonal reference frame (t_c, \mathbf{x}) :

$$ds^2 = (1 - 2\delta_p) dt_c^2 - \mathbf{a}^2 (\delta_{ij} - 2\mathcal{B}_{,ij}) dx^i dx^j, \quad (89)$$

where

$$u^\mu = (1 + \delta_p) \delta_0^\mu, \quad \mathcal{B} \equiv \int \mathbf{q} \frac{d\eta}{a^2 H}, \quad \mathbf{a} \equiv a \cdot (1 - A) = a_c \cdot (1 - q)$$

is the scalar scale factor. The proper time ds in geodesic $\mathbf{x} = \text{const}$ is connected to the comoving one, t_c , by the condition $ds = (1 - \delta_p) dt_c$.

The key equation (86) is the relativistic Poisson equation and links the Laplacian of gravity potential Φ with the comoving density perturbation $\delta\varepsilon_c$. Equation (88) represents the relativistic Euler equation, or Newton's second law. It connects the flow acceleration \dot{q} with the pressure gradient δp_c acting on it.

We have four gauge invariant scalars q , δ , δ_p and S , but the four metric potentials A , B , C , and D are not gauge invariant: any two of them can arbitrarily be chosen by appropriately selecting the functions X and Y (see footnote 21). Thus, in total we end with six independent scalars describing density perturbations in the Friedmann model. Gravitational equations (86)-(88) impose four constraints on the six potentials of an S mode. Apparently, the gravity equations alone are insufficient for describing the dynamics of S perturbations. One needs information on the physical state of matter in the form of two missing relations (equations of state). However, even without imposing constraints on the state of matter, we can derive general evolution

equations for the quasi-Friedmann model, similar to the Friedmann equations in the homogeneous cosmology.

In order to describe the geometry of weakly inhomogeneous flows, let us use scalar variables, including *both orders* (the zeroth and first) of perturbation theory. For the matter, these are the scalars of total density ε and pressure p , while for the metric they are the scalar scale factor \mathbf{a} and the Hubble function H_v of the volume expansion. Their relationship is defined as

$$H_v \equiv \frac{\dot{b}}{b} = \frac{1}{3} u^\mu{}_{;\mu} = u^\mu (\ln a_v)_{,\mu} \quad (90)$$

(the dot above a letter denotes a partial derivative over t_c), where we have introduced the following factors of medium volume expansion:

$$a_v \equiv \mathbf{a} \det^{1/3}(\delta_{ij} - \mathcal{B}_{,ij}) = b \cdot (1 - q), \quad b \equiv a_c \cdot (1 - \Delta\mathcal{B}/3). \quad (91)$$

The generalized Friedmann equation (21) for a weakly inhomogeneous Universe follows after direct summation of the first equations (82) and (86) and grouping terms in the function H_v and ε . The other equation (23) follows from Eqn (77) with account for the relationship $\varepsilon + p_{\text{tot}} = (1 + \delta_p)(\varepsilon + p_v)$.

Consider the structure of quasi-Hubble flow. According to Eqn (89), the proper distance between two neighboring medium elements, separated by coordinates δx^i , is given by

$$\delta r_i = \mathbf{a} (\delta_{ij} - \mathcal{B}_{,ij}) \delta x^j, \quad \det \left(\frac{\delta r_i}{\delta x^j} \right) = a_v^3. \quad (92)$$

Differentiating δr_i over the proper time s , we obtain the field of paired velocities of matter motion in the weakly inhomogeneous Universe:

$$\delta V_i \equiv \frac{\partial \delta r_i}{\partial s} = H_{ij} \delta r^j, \quad H_v = \frac{1}{3} H_i^i, \quad (93)$$

$$H_{ij} \equiv H_c \delta_{ij} - h_{ij}, \quad H_c = \frac{\dot{a}_c}{a_c}, \quad h_{ij} = \frac{1}{a^2 H} \mathfrak{q}_{,ij},$$

where H_{ij} is the matrix of gauge invariant Hubble functions describing the recession of matter in space. Only one feature here reminds us of the Hubble expansion: the relative recessional velocity for points of the medium is proportional to the distance between them. Yet these velocities are anisotropic and depend on spatial location.

B. Dynamics of cosmological scalar perturbations

If motions of quasi-Hubble flow obey Friedmann equation (21), then the cosmological perturbations behave as oscillators. In order to derive the evolution equation for the adiabatic scalar q , we write the general relationship between perturbations of comoving pressure and matter energy density in the following form:

$$\delta_p = \beta^2 \delta + \hat{\delta}_p, \quad (94)$$

where the function β^2 describes the speed squared at which scalar perturbations propagate in the medium (the speed of sound). For the Pascal media ($S = 0$), it is as follows:

$$\beta^2 = \sum_{m,l} f_m \beta_{ml}^2, \quad (95)$$

where β_{ml}^2 is the acoustic matrix of linear medium perturbations.²² The scalar of *isometric* pressure perturbation $\hat{\delta}_p$ describes the part of pressure which is not related to perturbations of the total energy density δ . Indeed, if initially only adiabatic perturbations are present, then $\hat{\delta}_p = 0$, and for $\delta = 0$, one finds $\delta_p = \hat{\delta}_p$. The relationship between $\hat{\delta}_p$ and field variables of medium components depends on the equation of state of matter.

From relationships (88) and (94) it follows that

$$\delta \varepsilon_c \equiv (\varepsilon + p) \delta = \alpha^2 H \left(\dot{q} - H \hat{\delta}_p \right), \quad (97)$$

$$\alpha^2 = \frac{\varepsilon + p}{H^2 \beta^2} = \frac{\gamma}{4\pi G \beta^2}.$$

Substituting these formulas into the Poisson equation (86), we arrive at

$$\alpha^2 a^3 \left(\dot{q} - H \hat{\delta}_p \right) = \int \alpha^2 \beta^2 \Delta q \frac{da}{H}.$$

²²It connects partial amplitudes of comoving perturbations of pressure and matter density, $\delta_p^{(m)} = \beta_{ml}^2 \delta_\varepsilon^{(l)}$, and the following relationships hold true (see Chapter 6 in book [2] for details):

$$f_m \beta_{ml}^2 = f_l \beta_{lm}^2, \quad f_l \beta^2 + \bar{f}_l = \sum_m f_m \beta_{ml}^2, \quad \sum_m \bar{f}_m = 0. \quad (96)$$

Direct differentiation of this relationship provides the equation for q [2]:

$$\ddot{q} + \left(3H + 2\frac{\dot{\alpha}}{\alpha}\right)\dot{q} - \beta^2\frac{\Delta q}{a^2} = I(\hat{\delta}_p, S), \quad (98)$$

$$I = I(\hat{\delta}_p, S) = \frac{(\alpha^2 a^3 H \hat{\delta}_p)'}{\alpha^2 a^3} - \frac{\Delta S}{4\pi G \alpha^2 a^2}.$$

On the left-hand side of equation (98), we have the acoustic d'Alambert operator for the scalar q describing the general adiabatic density perturbation. The right-hand side contains the source of dynamic action of isometric perturbation modes on the evolution of q . For an ideal Pascal media ($S = 0$), a more compact form of equation follows:

$$\frac{[\gamma a^2 \beta^{-2} (q' - \bar{H} \hat{\delta}_p)]'}{\gamma a^2} - \Delta q = 0, \quad (99)$$

where the prime stands for the derivative over the conformal time η , and $\bar{H} = aH$.

Equations (98) and (99) are valid for a broad variety of media (in particular, for fundamental scalar fields). We did not refer to the information on the microscopic structure of matter. The only geometric characteristic of a medium needed for the derivation of key equation (98) is β^2 , the mean velocity squared of propagation of scalar perturbations in the medium (95). Neglecting isometric perturbations (for example, in the case of a single medium, matter and Λ -term, and others), $\hat{\delta}_p = 0$ and the equation for q acquires a closed form [10, 11]:

$$\ddot{q} + \left(3H + 2\frac{\dot{\alpha}}{\alpha}\right)\dot{q} - \beta^2\frac{\Delta q}{a^2} = 0. \quad (100)$$

C. Eulerian coordinates and the Newton limit

The Eulerian reference frame (τ, \mathbf{y}) is uniquely set by the conditions $B = C = 0$ and is of interest, in particular, because the *peculiar* velocity of matter

$$\mathbf{v}_{\text{pec}} \equiv -\frac{\nabla v}{a} = -\frac{\nabla \mathbf{q}}{H}, \quad u_\mu = (1 + \Psi, v, i), \quad (101)$$

where $v = \mathbf{q}/H$, $\Psi = \Phi - S$, is defined relative to this grid. From the relationship between Lagrangian and Eulerian coordinates:

$$\tau \equiv t_E = t_c - v, \quad \mathbf{y} = \mathbf{x} + \mathbf{S}, \quad (102)$$

we obtain the metric tensor in the Eulerian representation:

$$ds^2 = (1 + 2\Psi) d\tau^2 - \mathbf{a}^2 d\mathbf{y}^2, \quad (103)$$

where $\mathbf{S} = -\nabla \mathcal{B}$ is the displacement vector of a medium element relative to its initial position. Apparently, the metric in the Eulerian coordinate system is independent of the gradients of potential q , and the scalar scale factor

$$\mathbf{a} = a(\tau) \cdot (1 - \Phi) \quad (104)$$

fully describes the locally isotropic observer space filled with inhomogeneous-matter. Metric (103) is the relativistic limit of the weak field in the Friedmann model, and for the nonrelativistic substance ($|S/\Phi| \ll 1$) we obtain the Newtonian limit $\Psi = \Phi$.

Since the curvature scalar and gravitational potential are small ($q \sim \Phi \lesssim 10^{-5}$) in the real Universe within the observed structure scale, we can drop terms v , Ψ , and Φ in Eqns (102)-(104), respectively, and introduce the physical Eulerian coordinate for the position of medium points $\mathbf{r} \simeq a \mathbf{y}$. Hence we obtain a convenient approximation for the description of the quasilinear stage of structure formation in the Universe:

$$\mathbf{r} = (1 + z)^{-1}(\mathbf{x} + \mathbf{S}), \quad \mathbf{v}_{\text{pec}} = \dot{\mathbf{r}} - H\mathbf{r} = a\dot{\mathbf{S}}. \quad (105)$$

Under the additional assumption of the smallness of the speed of sound, from equation (100) it follows that $q \simeq q_0 = q_0(\mathbf{x})$. Substituting it into formula (105), we obtain the Zel'dovich approximation (see Ref. [1] for more detail):

$$\mathbf{S} = -g \nabla q_0, \quad \mathbf{v}_{\text{pec}} = -\nu \nabla q_0, \quad \delta = g \Delta q_0, \quad \Phi = \phi q_0, \quad (106)$$

where the growth factors are introduced [see Eqn (12)]. They depend only on time and the relationship $a\phi/g = 3\Omega_m H_0^2/2 = \text{const}$ holds true.

References

- [1] Doroshkevich A G, Lukash V N, Mikheeva E V *Usp. Fiz. Nauk* **182** 3 (2012) [*Phys. Usp.* **55** (1) (2012)]
- [2] Lukash V N, Mikheeva E V *Fizicheskaya Kosmologiya* (Physical Cosmology) (Moscow: Fizmatlit, 2010)
- [3] Tinker J L et al. *Astrophys. J.* **724** 878 (2010)
- [4] Hufenberger K M, Seljak U *Mon. Not. R. Astron. Soc.* **340** 1199 (2003)
- [5] Zel'dovich Ya B *Astrofizika* **6** 319 (1970) [*Astrophysics* **6** 164 (1970)]
- [6] Press W H, Schechter P *Astrophys. J.* **187** 425 (1974)
- [7] Sachs R K, Wolfe A M *Astrophys. J.* **147** 73 (1967)
- [8] Harrison E R *Phys. Rev. D* **1** 2726 (1970)
- [9] Zeldovich Ya B *Mon. Not. R. Astron. Soc.* **160** 1P (1972)
- [10] Lukash V N *Pis'ma Zh. Eksp. Teor. Fiz.* **31** 631 (1980) [*JETP Lett.* **31** 596 (1980)]
- [11] Lukash V N *Zh. Eksp. Teor. Fiz.* **79** 1601 (1980) [*Sov. Phys. JETP* **52** 807 (1980)]
- [12] Sylos Labini F, Visilyev N L, Baryshev Y V *Astron. Astrophys.* **496** 7 (2009); arXiv:0902.0229v1
- [13] Lukash V N, Rubakov V A *Usp. Fiz. Nauk* **178** 301 (2008) [*Phys. Usp.* **51** 283 (2008)]
- [14] Karachentsev I D et al. *Astron. Astrophys.* **398** 479 (2003); arXiv:astro-ph/0211011v1
- [15] Komatsu E et al. *Astrophys. J. Suppl.* **192** 18 (2011); arXiv:1001.4538v3
- [16] Bertschinger E et al. *Astrophys. J.* **364** 370 (1990)
- [17] Kashlinsky A et al. *Astrophys. J. Lett.* **712** L81 (2010); arXiv:0910.4958v3

- [18] Lukash V N, Pilipenko S V *Astron. Zh.* **88** 611 (2011) [*Astron. Rep.* **55** 561 (2011)]
- [19] Huterer D *Gen. Relat. Grav.* **42** 2177 (2010); arXiv:1001.1758v3
- [20] Percival W J et al. *Mon. Not. R. Astron. Soc.* **381** 1053 (2007)
- [21] Granett B R, Neyrinck M C, Szapudi I *Astrophys. J.* **701** 414 (2009); arXiv:0812.1025v2
- [22] Jackson J C, Jannetta A L *JCAP* (11) 002 (2006); arXiv:astro-ph/0605065v2
- [23] Krichbaum T P et al. *Astron. Astrophys.* **329** 873 (1998)
- [24] Homan D C, Wardle J F C *Astrophys. J.* **535** 575 (2000); arXiv:astro-ph/0001298v1
- [25] Zhang Y-W, Fan J-H *Chin. J. Astron. Astrophys.* **8** 385 (2008)
- [26] Conroy C et al. *Astrophys. J.* **635** 990 (2005); arXiv:astro-ph/0508250v2
- [27] Kauffmann G *Mon. Not. R. Astron. Soc.* **274** 153 (1995); arXiv:astro-ph/9409075v1
- [28] Kauffmann G, Haehnelt M *Mon. Not. R. Astron. Soc.* **311** 576 (2000); arXiv:astro-ph/9906493v1
- [29] Navarro J F, Frenk C S, White S D M *Astrophys. J.* **490** 493 (1997); arXiv:astro-ph/9611107v4
- [30] Maoz D *Astrophys. J. Lett.* **490** L135 (1997); arXiv:astro-ph/9704173v2
- [31] Peebles P J E, Dicke R H *Astrophys. J.* **154** 891 (1968)
- [32] Bullock J S, Kravtsov A V, Weinberg D H *Astrophys. J.* **548** 33 (2001); arXiv:astro-ph/0007295v1
- [33] Lokas E L, Hoffman Y, in *Proc. of the 3rd Intern. Workshop on the Identification of Dark Matter* (Eds N J C Spooner, V Kudryavtsev) (Singapore: World Scientific, 2001) p.121; arXiv:astro-ph/0011295v1

- [34] Sheth R K, Tormen G *Mon. Not. R. Astron. Soc.* **308** 119 (1999); arXiv:astro-ph/9901122v2
- [35] Arkhipova N A et al. *Astron. Zh.* **84** 874 (2007) [*Astron. Rep.* **51** 787 (2007)]
- [36] Malinovsky A M, Lukash V N, Mikheeva E V *Astron. Zh.* **85** 675 (2008) [*Astron. Rep.* **52** 607 (2008)]
- [37] Girardi M et al. *Astrophys. J.* **505** 74 (1998); arXiv:astro-ph/9804187v1
- [38] Girardi M et al. *Astrophys. J.* **506** 45 (1998); arXiv:astro-ph/9804188v2
- [39] Tinker J et al. *Astrophys. J.* **688** 709 (2008); arXiv:0803.2706v1